

From Effective Lagrangians, to Chiral Bags, to Skyrmions with the Large- N_c Renormalization Group

NICHOLAS DOREY

Physics Department, University College of Swansea
Swansea SA2 8PP UK `pydorey@swansea.ac.uk`

and

MICHAEL P. MATTIS

Theoretical Division T-8, Los Alamos National Laboratory
Los Alamos, NM 87545 USA `mattis@skyrmion.lanl.gov`

We explicitly relate effective meson-baryon Lagrangian models, chiral bags, and Skyrmions in the following way. First, effective Lagrangians are constructed in a manner consistent with an underlying large- N_c QCD. An infinite set of graphs dress the bare Yukawa couplings at *leading* order in $1/N_c$, and are summed using semiclassical techniques. What emerges is a picture of the large- N_c baryon reminiscent of the chiral bag: hedgehog pions for $r \geq \Lambda^{-1}$ patched onto bare nucleon degrees of freedom for $r \leq \Lambda^{-1}$, where the “bag radius” Λ^{-1} is the UV cutoff on the graphs. Next, a novel renormalization group (RG) is derived, in which the bare Yukawa couplings, baryon masses and hyperfine baryon mass splittings run with Λ . Finally, this RG flow is shown to act as a *filter* on the renormalized Lagrangian parameters: when they are fine-tuned to obey Skyrme-model relations the continuum limit $\Lambda \rightarrow \infty$ exists and is, in fact, a Skyrme model; otherwise there is no continuum limit.

1. Introduction

1.1. *Effective hadron Lagrangians versus Skyrmions*

In the absence of reliable quantitative methods for computing the low-energy properties of QCD, a wide variety of phenomenological models of the nucleon have emerged and flourished. One general class of models, which predates QCD by some 30 years, starts from an *effective Lagrangian* for the baryon and meson fields. The hope in this approach is that the relevant physics is contained in the complete set of hadron Feynman diagrams. An orthogonal approach, pioneered by Skyrme in the early 1960s, uses topology: the baryon is viewed as a soliton, or *Skyrmion*, in the field of mesons [1,2].

On the face of it, the two approaches could not be more opposite. Baryon number in an effective quantum field theory of hadrons is simply the Noether charge associated with a $U(1)$ symmetry of the Lagrangian. In contrast, in the Skyrmion picture, baryon number is not associated with any continuous symmetry but is instead a topological invariant: the *winding number* of a meson field configuration. And the physics of Skyrmions is expressed, not in the language of Feynman diagrams, but in vocabulary more appropriate to solitons and other extended objects: collective coordinate quantization, symmetry classification of small fluctuations about the soliton, and so forth.

In this paper, we exhibit a precise connection between these two disparate approaches (see Fig. 1). The bridge between them is built by combining in a new way two important theoretical constructs: 't Hooft's $1/N_c$ expansion [3], N_c being the number of colors in the underlying gauge theory, and Wilson's renormalization group [4]. The parameter governing the flow of this so-called *large- N_c renormalization group* [5] is an ultraviolet cutoff $\Lambda \sim N_c^0$ which regulates the divergences in the effective Feynman diagrams. Our main result is that soliton models and (suitably fine-tuned) effective Lagrangian models are *completely equivalent* at leading order,¹ in the “continuum limit” $\Lambda \rightarrow \infty$ (to borrow lattice terminology). In this Section we introduce the key ideas behind the large- N_c renormalization group; the remainder of the paper is primarily devoted to exhibiting its solutions in a series of simple models.

¹ From now on, “leading order” refers to the $1/N_c$ expansion. The need to fine-tune the renormalized Lagrangian couplings is explained in Sec. 1.4 below.

1.2. The large- N_c limit and semiclassical physics

In 't Hooft's original formulation, the $1/N_c$ expansion is studied directly in QCD; as $N_c \rightarrow \infty$ the physics is dominated by the quenched planar quark-gluon graphs. But the large- N_c limit is actually much more predictive when the lessons of planar QCD are implemented, not at the fundamental quark-gluon level, but rather at the level of phenomenological models such as above. Thus, on the one hand, in effective hadron Lagrangians, it implies a set of *large- N_c selection rules* which place powerful constraints on the allowed particle spectrum and couplings contained in one's model. As examples of such rules [7,8], whereas meson masses typically scale like N_c^0 , baryons (being made up of N_c quarks) have masses that grow linearly with N_c . And whereas Yukawa couplings are strong, growing like $\sqrt{N_c}$, meson self-interactions are weak, with n -meson vertices disappearing like $N_c^{1-n/2}$. The complete set of these large- N_c selection rules is reviewed at the beginning of Sec. 2 below. On the other hand, in Skyrmon physics, $1/N_c$ plays an ostensibly different role, which is more easily summarized: it parametrizes the *semiclassical* expansion about the soliton. This is because $1/N_c$ always enters into Skyrmon Lagrangians in the combination \hbar/N_c .

In fact, this difference is illusory: the effective Lagrangian approach, too, becomes semiclassical in the large- N_c limit (a key to the equivalence of the two pictures). What we mean by this is twofold. First, in calculating the leading-order contribution to meson-baryon Green's functions, the naive, graph-by-graph, perturbative method fails, and one is forced instead to sum an infinite class of diagrams. Second, this sum may be accomplished by solving *classical* equations of motion for the meson fields in the background of the baryon source.

In order that these two points be understood, let us be very explicit at this stage, and in so doing, introduce the central field-theoretic problem of this paper. Consider the bare Yukawa coupling g_{bare} depicted in Fig. 2a, which scales like $\sqrt{N_c}$ as stated above. In principle, we would like to sum all radiative corrections to this vertex such as Figs. 2b-d, and thereby extract the renormalized Yukawa coupling g_{ren} , to leading order in $1/N_c$.² Focus first on Fig. 2b. It contains two factors of g_{bare} , therefore two factors of $\sqrt{N_c}$, as well as a 3-meson vertex which goes like $1/\sqrt{N_c}$; so this graph too scales like $\sqrt{N_c}$, and is a

² The calculation of renormalized single-meson emission/absorption from the nucleon is the simplest arena for our semiclassical methods, which may also be applied to more complicated processes such as meson-baryon and baryon-baryon scattering [5,9].

leading-order correction to g_{bare} . Likewise Fig. 2c scales like $\sqrt{N_c}$, as the reader can check by multiplying all vertices together. An example of a subleading correction is Fig. 2d. Unlike the others it contains a purely mesonic loop (indicated by the arrow), hence two extra factors of $1/\sqrt{N_c}$ uncompensated by extra Yukawa vertices. So Fig. 2d and the like are $1/N_c$ corrections, and will not concern us further.

A moment’s thought confirms the rule: the leading-order dressings are the *infinite set* of diagrams which contain only meson *trees* if the baryon line is erased. And the sum of all trees—like a soliton—is given by the solution to a classical equation of motion, which we write down in Sec. 3 below. The role of the bare large- N_c baryon in this equation is that of a heavy, slow-moving source, smeared out over a length-scale Λ^{-1} so as to cut off the short-distance divergences in the original Feynman graphs. As we shall see, the solution of the regulated equation is a hedgehog cloud of pions and/or other mesons for $r \geq \Lambda^{-1}$, glued onto the bare nucleon degrees of freedom which are restricted to $r \leq \Lambda^{-1}$. The energy of this cloud renormalizes the mass of the baryon ($M_{\text{bare}} \rightarrow M_{\text{ren}}$) while its large-distance behavior determines the physical Yukawa coupling ($g_{\text{bare}} \rightarrow g_{\text{ren}}$).

1.3. Of chiral bags and Cheshire cats

The resulting picture of the meson-dressed large- N_c baryon is highly reminiscent of yet a third class of phenomenological models, the *chiral bag models* [10–13]. These, too, are hybrid descriptions of the dressed baryon, in which explicit quark (rather than nucleon) degrees of freedom inside a bag of radius R are matched onto an effective theory of hedgehog pions outside the bag. Even this presumably important distinction between ‘nucleon’ versus ‘quark’ degrees of freedom inside the bag disappears as $N_c \rightarrow \infty$.³ For, in this limit, the N_c quarks may be treated in Hartree approximation, and their individual wave functions effectively condense into a common mean-field wave function, which we may identify with the “wave function of the nucleon.” Outside the bag, the analogy is closer still: the pion field configuration is again determined by solving a nonlinear field equation coupled to a static source at $r = R$. The only significant difference between our composite meson-dressed large- N_c baryon and the traditional chiral bag is this: our composite baryon

³ This observation was originally made by Witten (Ref. [8], Secs. 5 and 9), and exploited by Gervais and Sakita (Ref. [14], Sec. V). These two papers are highly recommended background reading, as they too are concerned primarily with the semiclassical nature of large- N_c . In particular Gervais and Sakita were the first to study chiral-bag-type structures in this limit, although not from our effective hadron Lagrangian starting point.

follows solely from large N_c and has *nothing whatsoever to do with chiral symmetry!* For this reason we shall refer to it as a “chiral bag” (Fig. 1 again), being careful to retain the quotation marks to avoid confusion with the traditional chiral bag.

Associated with the traditional chiral bag in the recent literature is the so-called *Cheshire cat principle* [15,13], which states that physical quantities should be independent of the size and shape of the bag. This proposal is motivated by the success of bosonization in 1+1 dimensions, which provides an exact mapping between, for instance, the elementary fermion of the massive Thirring model and the soliton of the sine-Gordon equation [16]. In its most extreme form, it implies that R can safely be set to zero, yielding a description of the nucleon purely in terms of pion fields. One may conjecture that this limit is nothing other than the Skyrme model [12,13]. However, since no equivalent of bosonization has been made to work in 3+1 dimensions, the theoretical status of the Cheshire cat principle has remained uncertain.

From our present large- N_c perspective, the bag radius R is best reinterpreted as the short-distance cutoff Λ^{-1} of the large- N_c effective theory. It is then easy to see the significance of the Cheshire cat principle: the cutoff-independence of physical quantities is usually referred to as renormalization group invariance [4]. However, except in special cases, renormalization group invariance of the physical masses and couplings never comes for free; the corresponding bare quantities must be varied simultaneously with the cutoff. As stated earlier, we will refer to this program as the *large- N_c renormalization group*, and devote considerable space to mapping out its solutions. To our understanding, the concept of such a flow is not only absent from the usual Cheshire cat philosophy, but in fact orthogonal to it; R in that scheme is nothing more than a gauge-fixing parameter.

1.4. The large- N_c renormalization group as a “filter”

The limit of zero bag size, $R \rightarrow 0$ or $\Lambda \rightarrow \infty$, corresponds to removing the cutoff completely. This continuum limit, if it can be taken at all, is by definition a UV stable fixed point of the renormalization group flow.⁴ In light of the above discussion, it is natural to conjecture that such a fixed point exists if and only if the homogeneous meson

⁴ Because we are implementing renormalization group invariance strictly at leading order in $1/N_c$, the limit $\Lambda \rightarrow \infty$ is to be taken *after* $N_c \rightarrow \infty$. We suspect that these limits do not commute.

field equations (*i.e.*, with the baryonic source set to zero) supports a soliton solution.⁵ Thus we propose that variants of the Skyrme model describe the possible continuum limits of effective Lagrangian theories of mesons and baryons in the large- N_c limit.

On reflection, there is an obvious counting problem with this scenario: effective Lagrangians always contain more free parameters than the corresponding soliton models. Thus, in the former, the physical masses and couplings are all independent, while in the latter, there exist non-trivial relations among them; for instance, the Yukawa constant g_{ren} is completely determined by the meson self-couplings [2]. (This feature, of course, is *precisely the point* of the Skyrme approach.) If our proposal is correct, it follows that unless the renormalized parameters in the effective Lagrangian are tuned *exactly* to those of the corresponding soliton model, there must be some mathematical obstacle to taking the continuum limit. In other words, we conjecture that the large- N_c renormalization group acts as a *filter*, blocking the path to the continuum except for a measure-zero subset of the space of renormalized parameters. This filter idea is the central theme of this paper, and is explicitly realized in the models to follow. The attentive reader will recognize in the phrasing of this counting problem the classic symptom of the existence of an “irrelevant operator” [4]; naturally this operator turns out to be the bare Yukawa coupling itself.

1.5. The plan of this paper

The paper is organized as follows. Sections 2 and 3 recapitulate our recent Letter [5], in somewhat more detail, and at a more leisurely pace. (Independently, Manohar [17] has reached similar conclusions to Ref. [5]; other relevant precursors are Refs. [9] and [14].) In particular, Sec. 2 reviews the large- N_c selection rules mentioned above, and gives the recipe for constructing large- N_c -compatible effective Lagrangians. Section 3 is devoted to semiclassics: the problem posed in Fig. 2 is solved completely at a formal level, the issue of meson contributions to the baryon self-energy is examined, the hedgehog structure of the meson cloud is revealed, and the large- N_c renormalization group is defined.

The reader already familiar with the contents of Ref. [5] is encouraged to skip directly to Secs. 4-8, in which the large- N_c renormalization group is applied to a series of effective hadron models. What distinguishes these models from one another is our choice of the purely mesonic piece of the action, $\mathcal{L}_{\text{meson}}$. In Sec. 4, $\mathcal{L}_{\text{meson}}$ is simply the

⁵ The only exception we have found to this rule is a theory of non-self-interacting mesons (Sec. 4).

free pion Lagrangian. Not surprisingly, one finds essentially no running of the bare πN Yukawa coupling: $g_{\text{bare}}(\Lambda) \cong g_{\text{ren}}$. Much more interesting is the model of Sec. 5, in which $\mathcal{L}_{\text{meson}} = \frac{f_\pi^2}{16} \text{Tr} \partial_\mu U^\dagger \partial^\mu U$, the leading term in chiral perturbation theory. This is a clean initial test of the “filter” idea conjectured above, because this model is known *not* to support a soliton, thanks to Derrick’s theorem [18]. And indeed, we discover a critical value of the cutoff, $\Lambda_{\text{crit}} \cong 340 \text{ MeV}$, beyond which the large- N_c renormalization group cannot be pushed. In Sec. 6 we construct an *analytically soluble* 2+1 dimensional model, in which the would-be Skyrme is simply the *instanton* of the $O(3)$ σ model in one lower dimension. In this model the physics is all that one might have hoped: unlike Sec. 5 there is no ultraviolet obstruction to the large- N_c renormalization group; the bare coupling $g_{\text{bare}}(\Lambda)$ is irrelevant, flowing to zero like Λ^{-4} ; and a “toy” Skyrme model indeed lies at the end of the large- N_c renormalization group trajectory, at which point explicit baryon number effectively transmutes into the winding number of the meson cloud.

Finally, in Secs. 7-8 we augment the nonlinear pion Lagrangian of Sec. 5 with the 4-derivative “Skyrme term” and study the large- N_c renormalization group, both in the measure-zero case when the physical Yukawa coupling is tuned precisely to its Skyrme-model value (Sec. 7), and in the generic case when they differ (Sec. 8). In a surprising way, involving essential singularities in Skyrme’s equation, and *local instabilities* that develop in the pion cloud for $\Lambda \geq \Lambda_{\text{crit}}$ (see the Appendix for technical details), our “filter” conjecture is borne out.

In light of this already long Introduction, we will spare the reader a Conclusions section, and commend him instead to keep the “large- N_c renormalization group as filter” idea firmly in mind as he works his way through the examples.

2. Constructing large- N_c effective Lagrangians

2.1. Large- N_c selection rules

As mentioned in Sec. 1, the large- N_c limit imposes several stringent requirements on the allowed spectrum and interactions of hadrons, which we now review. These rules can be derived quite independently from several different approaches: not just a planar-diagrammatic analysis of large- N_c QCD [7,8,19,20] but also the Hartree approximation originally employed by Witten [8], the Skyrme model [2,14,21], the non-relativistic quark model [22–24], and finally the self-consistency of the effective hadron Lagrangian [14,25] as recently emphasized in a series of interesting papers by Dashen, Jenkins and Manohar

[26,27]. The following rules (the first two of which were already invoked in Sec. 1) should be considered robust, model-independent features of the large- N_c limit:

(i) As noted originally by Veneziano, purely mesonic vertices with n external legs scale like $N_c^{1-n/2}$ [7,8]. An important example with $n = 1$ is that the pion decay constant $f_\pi \sim \sqrt{N_c}$, whereas meson masses ($n = 2$) generically scale like N_c^0 .

(ii) Vertices with two baryon legs and n meson legs also scale like $N_c^{1-n/2}$ so that baryon masses ($n = 0$) and Yukawa couplings ($n = 1$) grow like N_c and $\sqrt{N_c}$, respectively [8,14,19,20].

(iii) The 2-flavor stable baryon spectrum of large- N_c QCD (with N_c odd) consists of an infinite tower of positive parity states with $I = J = \frac{1}{2}, \frac{3}{2}, \frac{5}{2}, \dots$.⁶ To leading order these states are degenerate [2,14,19,20,26], with bare mass $M_{\text{bare}} \sim N_c$ (as baryons are made of N_c quarks). Hyperfine baryon mass splittings have the form $J(J+1)/2\mathcal{I}_{\text{bare}}$ where $\mathcal{I}_{\text{bare}} \sim N_c$ [2,19,20,27]. In the Skyrme model these states correspond to (iso)rotational excitations of the static hedgehog and the splitting term corresponds exactly to the rotational kinetic energy of the Skyrmion [2].

(iv) In contrast, the spatial extent of a baryon does not grow but has a smooth N_c -independent limit as $N_c \rightarrow \infty$ as do the various baryon form factors such as electromagnetic charge distributions, and baryon number density itself [8,2].

(v) Yukawa couplings are constrained to obey the “proportionality rule” which fixes the interaction strength of a given meson with each member of the baryon tower as a multiple of one overall coupling constant [2,14,21,23,26] (e.g., $g_{\pi NN} \propto g_{\pi N\Delta} \propto g_{\pi\Delta\Delta} \dots$), up to corrections of order $1/N_c^2$ [26].

(vi) Finally, the allowed couplings of mesons to the baryon tower must obey the $I_t = J_t$ rule [21,23,25]. For example the ρ meson must be tensor-coupled to the nucleon while the ω meson is vector-coupled at leading order in $1/N_c$ [25,20,24], in good agreement with phenomenology [28]. When crossed from the t -channel to the s -channel, this rule also implies nontrivial model-independent relations among meson-baryon S matrix elements [29–31], which are tested against the experimental data in Refs. [30–31].⁷

⁶ In the Skyrme-model representation this tower is truly infinite whereas in the quark-model representation it tops off at $N_c/2$; see Ref. [24] for a detailed discussion of how to translate Skyrme-model operators into quark-model operators and *vice versa* in light of this difference.

⁷ Rules (v) and (vi) are elementary examples of “large- N_c group theory,” the state-of-the-art phenomenological predictions of which are summarized in Ref. [24]. The existence of such group-theoretic relations may be traced to the fact that $SU(2N_F)$ spin \times flavor symmetry becomes exact

These selection rules must be implemented in any large- N_c -compatible effective hadron Lagrangian. What we stressed in our Letter [5] and will review below is the *consistency* of these rules, meaning that once they are incorporated into the bare Lagrangian they continue to hold for physical, renormalized quantities as well. Thus, while the baryon mass spectrum is renormalized at leading order by the interactions with the mesons, the $J(J+1)$ structure discussed in **(iii)** is preserved, and so, too, the form of the $\mathcal{O}(\sqrt{N_c})$ Yukawa couplings of the mesons to the baryon tower dictated by **(v)** and **(vi)**. And while the “bare” nucleon size (as given by the naive ultraviolet cutoff $\Lambda^{-1} \sim N_c^0$) is effectively enlarged by the meson cloud, it remains of order N_c^0 as per **(iv)**. This is because the spatial extent of the cloud is dictated by the parameters **(i)** of the meson Lagrangian, for instance m_ρ^{-1} , or the product of Skyrme-model parameters $(e_s f_\pi)^{-1}$ as we shall see in Secs. 7-8 below.

In general, an effective meson-baryon Lagrangian is a sum of four parts:

$$L_{\text{eff}} = L_{\text{baryon}} + L_{\text{meson}} + L_{\text{yukawa}} + L_{\text{seagull}} . \quad (2.1)$$

In light of the above selection rules, let us discuss, in turn, the proper construction of each of these parts.

2.2. Constructing L_{baryon} .

We start with a relativistic baryon Lagrangian for the tower described in **(iii)** above:

$$\bar{N}(i\gamma^\mu \partial_\mu - M_N)N + (\text{higher } I = J \text{ baryons}) \quad (2.2)$$

where N means $\binom{p}{n}$. We will need to recast this unwieldy infinite sum in a more useful form. Since large- N_c baryons are heavy, it is natural to split their propagators in the usual way into forwards-in-time (U -spinor) plus backwards-in-time (V -spinor) pieces. The latter account for the so-called Z -graph contributions to Feynman diagrams, which turn out to be subleading as we review momentarily (Sec. 2.5). The remaining time-ordered diagrammatics is one in which Z -graphs have been eliminated, and with them the higher components of the baryon-antibaryon Fock space. In this way, baryon *quantum field theory* collapses to baryon *quantum mechanics*. But we can simplify the physics even further. For

as $N_c \rightarrow \infty$ [14,26]. This is one of the two main attractions of large- N_c physics, the other being its amenability to a semiclassical treatment.

processes involving one baryon only, interacting with an arbitrary number of mesons, it is natural to work in or near the baryon’s rest frame, in which case, finally,

$$L_{\text{baryon}} = -M_{\text{bare}} + \frac{1}{2}M_{\text{bare}}\dot{\mathbf{X}}^2 + \mathcal{I}_{\text{bare}}\text{Tr}\dot{A}^\dagger\dot{A} + \dots, \quad (2.3)$$

the dots denoting $1/N_c$ corrections. The first two terms on the right-hand side are the usual nonrelativistic approximation to the relativistic mass-energy, $\mathbf{X}(t)$ being the baryon’s position.

The third term, the (iso)rotational kinetic energy, is perhaps less familiar. It represents free motion on the baryon’s spin/isospin manifold (just as the previous term denotes free spatial translation), with $A(t) \in SU(2)$ being the baryon’s spin/isospin collective coordinate. The full meaning of this term is revealed in the beautiful path integral identity due to Schulman [32]:

$$\begin{aligned} & \int_{A(t_1)=A_1}^{A(t_2)=A_2} \mathcal{D}A(t) \exp i \int dt (-M_{\text{bare}} + \mathcal{I}_{\text{bare}}\text{Tr}\dot{A}^\dagger\dot{A}) \\ &= \sum_{J=\frac{1}{2}, \frac{3}{2}, \dots} \sum_{i_z, s_z = -J}^J \langle A_2 |_{i_z s_z}^{I=J} \rangle e^{-i(t_2-t_1)M_{\text{bare}}^J} \langle I=J |_{i_z s_z} A_1 \rangle, \end{aligned} \quad (2.4)$$

where

$$M_{\text{bare}}^J = M_{\text{bare}} + \frac{J(J+1)}{2\mathcal{I}_{\text{bare}}}. \quad (2.5)$$

In other words, $\mathcal{I}_{\text{bare}}\text{Tr}\dot{A}^\dagger\dot{A}$ is convenient shorthand for the free propagation of an *infinite tower* of $I = J$ baryons with the mass spectrum of a rigid rotor—exactly as required by rule **(iii)** given above. We will adopt Skyrme-model nomenclature and refer to $\mathcal{I}_{\text{bare}}$ as the “bare moment of inertia” of the baryon [2]. The brackets

$$\langle A |_{i_z s_z}^{I=J} \rangle = (2J+1)^{1/2} (-)^{J-s_z} D_{-s_z, i_z}^{(J)}(A^\dagger) \quad (2.6)$$

in Eq. (2.4) are just the change-of-basis overlaps between the usual spin-isospin baryon representation (the nucleons with $I = J = \frac{1}{2}$, the Δ ’s with $I = J = \frac{3}{2}$, etc., with spin and isospin z components s_z and i_z), and baryon states $|A\rangle$ sharp instead in the spin/isospin collective coordinate. The $|A\rangle$ basis too, while popularized by the Skyrme model [2], is useful more generally in large- N_c physics [14,22,23].

2.3. Constructing L_{meson} .

As for the meson piece of the action, it is best to leave L_{meson} completely unspecified for the time being, subject only to the scaling rule **(i)** discussed above. Importantly, if one then rescales all meson fields by a mass parameter proportional to $\sqrt{N_c}$ (such as the pion decay constant f_π), a multiplicative factor of N_c/\hbar sits in front of the meson action. So a leading-order analysis in the $1/N_c$ expansion is tantamount to a *semiclassical* ($\hbar \rightarrow 0$) treatment of the mesonic part of the path integral. We will exploit this feature shortly.

2.4. Constructing L_{Yukawa} .

Next, consider L_{Yukawa} . For large N_c , the usual pseudovector coupling of the pion to the nucleon,⁸

$$g_{\pi NN}^{\text{bare}} \partial_\mu \vec{\pi} \cdot \bar{N} \gamma^\mu \gamma^5 \vec{\tau} N , \quad (2.7)$$

must be augmented by similar couplings to the entire $I = J$ tower of baryons in a manner fixed by the proportionality rule **(v)**. As before, the $|A\rangle$ basis for the baryons permits an especially compact representation of this set of couplings, namely [2,6]

$$3g_{\pi NN}^{\text{bare}} \frac{\partial}{\partial x^{l'}} \pi^a(x) D_{al}^{(1)}(\hat{A}(t')) \delta^3(\mathbf{x}') . \quad (2.8)$$

Here the primed space-time coordinate $x' = (t', \mathbf{x}')$ is the Poincaré transformation of x into the center-of-mass frame of the baryon, assumed to be moving with fixed velocity $\dot{\mathbf{X}}$ relative to the Lab frame; when $\dot{\mathbf{X}} \ll 1$ so that Lorentz contractions are irrelevant, one simply has

$$\mathbf{x}' \approx \mathbf{x} - \mathbf{X}(t) . \quad (2.9)$$

The rotation matrix $D^{(1)}(\hat{A})$ is an operator (hence the ‘hat’ on the A) on the spin and isospin quantum numbers of the single-baryon Hilbert space. It is completely specified by

⁸ We have absorbed the normally explicit factor of $(2M_N)^{-1}$ into the pseudovector coupling constant $g_{\pi NN}^{\text{bare}}$, which therefore has dimensions of length. The reason that pseudovector coupling is far preferable to pseudoscalar coupling in large- N_c physics is that the latter involves an awkward cancellation: γ^5 couples the ‘large’ to the ‘small’ components of the nucleon spinor, the ‘small’ components being down by $1/N_c$, which compensates the fact that the pseudoscalar constant grows like $N_c^{3/2}$ as dictated by the Goldberger-Treiman relation.

its matrix elements in the conventional spin-isospin baryon basis:

$$\begin{aligned}
\langle I'=J' \mid D_{al}^{(1)}(\hat{A}) \mid I=J \rangle_{i'_z s'_z i_z s_z} &= \langle I'=J' \mid D_{al}^{(1)}(\hat{A}) \int_{SU(2)} dA \mid A \rangle \langle A \mid I=J \rangle_{i'_z s'_z i_z s_z} \\
&= \int_{SU(2)} dA D_{al}^{(1)}(A) (2J'+1)^{1/2} (-)^{J'-s'_z} D_{-s'_z, i'_z}^{(J')*}(A^\dagger) \\
&\quad \times (2J+1)^{1/2} (-)^{J-s_z} D_{-s_z, i_z}^{(J)}(A^\dagger) \\
&= [(2J+1)(2J'+1)]^{1/2} (-)^{J'-J+s_z+i'_z} \\
&\quad \times \begin{pmatrix} 1 & J & J' \\ a & i_z & -i'_z \end{pmatrix} \begin{pmatrix} 1 & J & J' \\ l & -s_z & s'_z \end{pmatrix}.
\end{aligned} \tag{2.10}$$

To obtain the first equality we have inserted a complete set of $\mid A \rangle$ states on which $D_{al}^{(1)}(\hat{A})$ is sharp; the second equality follows from Eq. (2.6); and the third, from the textbook expression for the integral of three Wigner D -functions. The two resulting $3j$ symbols express conservation of isospin and angular momentum, respectively, while the overall square-root coefficient embodies the proportionality rule **(v)**.

It is easily checked that the terms in Eq. (2.7) involving the spatial derivatives of the pion are correctly reproduced by Eqs. (2.8) and (2.10), once one specializes to ‘in’ and ‘out’ nucleons by plugging in $J = J' = \frac{1}{2}$. In contrast, the time derivative of the pion has been dropped in moving from (2.7) to (2.8). This is because $\partial_0 \vec{\pi}$ multiplies the Dirac matrix $\gamma^0 \gamma^5$ which couples the ‘large’ components of the baryon’s Dirac spinor to the ‘small’ components, the latter being down by $v/c \sim 1/N_c$. As often happens, the $1/N_c$ expansion has broken apart a Lorentz-invariant quantity.

Beyond the nucleons, the coupling (2.8) contains useful phenomenological information about the higher $I = J$ baryons as well. Sandwiching it between nucleon and Δ states using Eq. (2.10), one calculates a $\Delta \rightarrow N\pi$ decay width within a few MeV of its experimental value of 120 MeV [2,6,33]. In the same way, one discovers that the higher baryons have widths so large ($\Gamma_{\frac{5}{2} \rightarrow \Delta\pi} \approx 800$ MeV, $\Gamma_{\frac{7}{2} \rightarrow \frac{5}{2} + \pi} \approx 2600$ MeV, $\Gamma_{\frac{9}{2} \rightarrow \frac{7}{2} + \pi} \approx 6400$ MeV, etc.) that they cannot sensibly be regarded as “particles” at all [6,33]. So these higher-spin states, the existence of which is often considered a major failing of the large- N_c approach, are actually *not* in conflict with phenomenology.⁹

⁹ The story of these unwanted large- N_c baryons is much more complicated in models with three or more light flavors. The 3-flavor Skyrme model [34], for example, predicts exotic baryons not just with high spin but also with *low* spin, for instance a spin- $\frac{1}{2}$ antidecuplet. In quark-model language such exotics map onto baryons with N_c quarks plus extra $q\bar{q}$ pairs [22]. Large- N_c

Like the pions, the allowed nucleon couplings of the ρ , ω and/or σ mesons (for example) must also be echoed by couplings to the entire $I = J$ tower [25]:

$$g_{\rho NN}^{\text{bare}} \partial_\mu \vec{\rho}_\nu \cdot \bar{N} \sigma^{\mu\nu} \vec{\tau} N \longrightarrow 3g_{\rho NN}^{\text{bare}} \epsilon_{ijk} \frac{\partial}{\partial x^{i'}} \rho_j^a(x) D_{ak}^{(1)}(A(t')) \delta^3(\mathbf{x}') \quad (2.11a)$$

$$g_{\omega NN}^{\text{bare}} \omega_\mu \bar{N} \gamma^\mu N \longrightarrow g_{\omega NN}^{\text{bare}} \omega^0(x) \delta^3(\mathbf{x}') \quad (2.11b)$$

$$g_{\sigma NN}^{\text{bare}} \sigma \bar{N} N \longrightarrow g_{\sigma NN}^{\text{bare}} \sigma(x) \delta^3(\mathbf{x}') \quad , \quad (2.11c)$$

again dropping Dirac structures that involve ‘small’ components. The N_c scalings are

$$g_{\pi NN}^{\text{bare}} \sim g_{\rho NN}^{\text{bare}} \sim g_{\omega NN}^{\text{bare}} \sim g_{\sigma NN}^{\text{bare}} \sim \sqrt{N_c} . \quad (2.12)$$

Conspicuously absent from this list of permitted Yukawa couplings are the *vector* coupling of the ρ meson and the *tensor* coupling of the ω meson, $g_{\rho NN}^{\text{vec}} \vec{\rho}_\mu \cdot \bar{N} \gamma^\mu \vec{\tau} N$ and $g_{\omega NN}^{\text{tens}} \partial_\mu \omega_\nu \bar{N} \sigma^{\mu\nu} N$. These alternative couplings are forbidden by rule **(vi)** given earlier, meaning that in contrast to (2.12),

$$g_{\rho NN}^{\text{vec}} \sim g_{\omega NN}^{\text{tens}} \sim \frac{1}{\sqrt{N_c}} \quad (2.13)$$

and we can forget about them. The incorporation of these additional mesons is deferred to future work;¹⁰ for simplicity the explicit meson models analyzed below will be built from pions alone.

counting implies that each such pair costs a factor of $1/\sqrt{N_c}$ to produce [3,8]. And indeed one can show that matrix elements of physically relevant operators between “normal” and “exotic” baryons are down precisely by $1/N_c^{k/2}$ where k is the number of such $q\bar{q}$ pairs; see Ref. [24], Sec. XIII for details.

¹⁰ A natural extension of the ideas in the present paper, and one more in keeping with Wilson’s original philosophy of the renormalization group [4], is to add more and more mesons to the model as the cutoff Λ is increased. This is consistent with the spectral representation of large- N_c physics, which requires, not just an infinite tower of baryons, but apparently also an infinite number of mesons in each channel [8]. The smearing of the baryon over a distance Λ^{-1} can then be thought of as being due to the interactions with mesons of mass greater than Λ , which are omitted from the model, whereas all mesons of mass less than Λ are explicitly kept.

2.5. Constructing L_{seagull}

Finally we discuss couplings such as Fig. 3a, in which more than one meson interacts with the baryon at the same space-time point. For want of a better word we refer to these vertices as “seagulls.” From QCD one can show that n -meson seagulls generically scale like $N_c^{1-n/2}$ (rule **(ii)** above). A familiar example from chiral perturbation theory is the coupling to the nucleon of the pion’s axial current, which is formed from the U field, $U = \exp(2i\vec{\pi} \cdot \vec{\tau}/f_\pi)$. Taylor expanding U gives coefficients proportional to $g_A f_\pi^{-n}$ for the n -pion couplings to the nucleon, where $n = 1, 3, 5, \dots$. Since $g_A \sim N_c$ and $f_\pi \sim \sqrt{N_c}$ these indeed have the full-strength scaling behavior with N_c . An exception to this scaling rule is the set of n -pion seagulls arising from the *vector* current coupling. These are proportional to $g_V f_\pi^{-n}$, $n = 2, 4, 6, \dots$, and since $g_V = 1$ by vector current conservation they all drop out as $N_c \rightarrow \infty$.

Quite aside from any “bare” seagulls that one may choose to include in the bare Lagrangian, one must also examine the *effective* seagulls that arise from the backwards-in-time baryons (Z -graphs), once a Feynman diagram is decomposed into a sum of time-ordered diagrams. Inevitably, these approximately pointlike induced vertices are termed “ Z -gulls.” As illustrated in Figs. 3b-c, they come from approximating the V -spinor propagator by the constant $-i/2M_{\text{ren}}$ up to nonlocal $\mathcal{O}(N_c^{-2})$ corrections, where M_{ren} is the physical baryon mass. Naively, the strength of the Z -gull in Fig. 3c is then $g_{\text{bare}}^2/M_{\text{ren}} \sim N_c^0$; since this is the same order as a full-strength 2-meson bare seagull, it appears such a vertex must be kept. However, this naive counting is *incorrect*.¹¹ The reason is easily seen by writing out the Feynman rules for the U and V spinors directly. For precisely those Yukawa couplings (2.8) and (2.11) permitted by the $I_t = J_t$ rule **(vi)**, there is an extra suppression of $\vec{\sigma} \cdot \mathbf{p}/M \sim 1/N_c$ at each of the two vertices in Fig. 3b. This is the cost of turning a U -spinor into a V -spinor or *vice versa*, when the meson coupling is dominantly block-diagonal in the Dirac space. We conclude that in self-consistent large- N_c models, Z -gulls are actually suppressed by two powers of $1/N_c$ compared with bare seagulls, and may safely be dropped.

For simplicity, in the explicit models analyzed below, we will choose to set to zero all bare seagulls as well. Instead we will focus on the renormalization of the Yukawa interaction and show that, in many cases, it corresponds to an irrelevant operator of the large- N_c renormalization group. We conjecture that in these cases the higher-point bare seagull couplings are also irrelevant operators, but we will leave this interesting question for future work.

¹¹ We are indebted to Jim Friar for pointing out an error in an earlier draft of this paper.

3. Large- N_c Semiclassical Analysis

3.1. Formal summation of the leading-order graphs

We now return to the central problem posed in Sec. 1, namely the summation of the leading-order contributions to the renormalized Yukawa constants g_{ren} . Recall from Fig. 2 that the leading-order graphs are those containing no purely mesonic loops, in other words, those graphs which would be meson trees if one were to erase the baryon line. The complete set of such graphs is captured in Fig. 4.

Not surprisingly, being tree-like, Fig. 4 can be generated as the solution to a classical equation of motion. As a concrete example, with pions only, suppose that

$$L_{\text{meson}} \equiv L_{\pi} = \frac{1}{2}(\partial_{\mu}\vec{\pi})^2 - \frac{1}{2}m_{\pi}^2\vec{\pi}^2 - V(\vec{\pi}) \quad (3.1)$$

where V contains the quartic and higher pion self-interactions. The pion trees with one external pion line sum to a quantity we call $\vec{\pi}_{\text{cl}}$ (the subscript ‘cl’ standing interchangeably for ‘classical’ or ‘cloud’) which solves the Euler-Lagrange equation implied by Eqs. (3.1) and (2.8):

$$(\square + m_{\pi}^2)\pi_{\text{cl}}^a(\mathbf{x}, t) + \frac{\partial V}{\partial \pi_{\text{cl}}^a} = 3g_{\pi NN}^{\text{bare}} D_{al}^{(1)}(A(t')) \frac{\partial}{\partial x^{l'}} \delta^3(\mathbf{x}'), \quad (3.2)$$

x' referring to the center-of-mass frame of the moving baryon as before. This equation is illustrated in diagrammatic form in Fig. 5. Comparing Fig. 5 with Fig. 4, we find apparent agreement, save for the “missing” sum over the $n!$ tanglings. But this sum is *already implicit* in Fig. 5. To see this, insert into the right-hand side of Fig. 5 the resolution of unity into a sum over all $n!$ (boosted) time orderings of the attachment points z_k ,

$$1 = \sum_{\rho \in S_n} \theta(z'_{\rho(2)}{}^0 - z'_{\rho(1)}{}^0) \theta(z'_{\rho(3)}{}^0 - z'_{\rho(2)}{}^0) \times \cdots \times \theta(z'_{\rho(n)}{}^0 - z'_{\rho(n-1)}{}^0), \quad (3.3)$$

ρ being a permutation, and for each element in this sum relabel $z_{\rho(k)} \rightarrow z_k$. In this way we recapture, not Fig. 4 precisely, but rather Fig. 6, which differs from Fig. 4 only in the time-ordering prescription up the baryon line. This difference is truly unimportant; backwards-in-time baryon propagation is always a $1/N_c$ effect.¹²

¹² In this particular instance the suppression of Z -graphs is even *greater* than that discussed in Sec. 2.5 above; shrinking a V -spinor propagator to a point here results in a meson loop, which itself is $1/N_c$ suppressed (see Fig. 2d).

To summarize, Eq. (3.2) correctly accounts for the leading-order contributions to the renormalized meson-baryon coupling, up to $1/N_c$ corrections. The answer is conveniently expressed as a *quantum mechanical* path integral over the baryon's translational and (iso)rotational collective coordinates:

$$\int \mathcal{D}A(t)\mathcal{D}\mathbf{X}(t) \pi_{\text{cl}}^a(\mathbf{x}, t) \exp i \int dt \left(L_{\text{baryon}} + L_{\text{meson}}[\vec{\pi}_{\text{cl}}] + L_{\text{Yukawa}}[\vec{\pi}_{\text{cl}}] \right), \quad (3.4)$$

ignoring seagulls for simplicity as stated above. Our progress to this point has been that the path integration over the field-theoretic variable $\vec{\pi}$ has been carried out in semiclassical approximation. This simply means replacing $\vec{\pi}$ by $\vec{\pi}_{\text{cl}}$ everywhere in (3.4), the justification being that $1/N_c$ always appears in the combination \hbar/N_c as highlighted earlier.

Thanks to the rescaling argument of Sec. 2.3, the meson cloud, like a skyrmion, is a nonperturbatively large configuration, scaling like $f_\pi \sim \sqrt{N_c}$, although its spatial extent goes like N_c^0 . Another general point: it is not sufficient that the cloud be a solution to the Euler-Lagrange equation; it must actually be a local *minimum*, in other words it must be locally stable against small deformations. This stability issue will reemerge in Sec. 8 below. The interesting related question, What does an unstable cloud collapse *into?*, is examined at the end of the Appendix.

3.2. Baryon self-energy and baryon-meson vertex corrections

What is the meaning of the terms $L_{\text{meson}}[\vec{\pi}_{\text{cl}}] + L_{\text{Yukawa}}[\vec{\pi}_{\text{cl}}]$ in Eq. (3.4)? Graphically, the answer can be seen in Fig. 7. As Fig. 7c in particular makes clear, these terms fully account for the meson-tree baryon self-energy and baryon-meson vertex corrections that we have neglected till now [19,27]. Taylor-expanding the exponential of these terms produces an arbitrary number of such insertions at all placements along the baryon line, automatically with the correct combinatorics. Moreover, since $\vec{\pi}_{\text{cl}}$ itself depends on the baryon collective coordinates $\mathbf{X}(t)$ and $A(t)$ through the Yukawa source on the right-hand side of (3.2), $L_{\text{meson}}[\vec{\pi}_{\text{cl}}] + L_{\text{Yukawa}}[\vec{\pi}_{\text{cl}}]$ have this dependence as well, and on general grounds must have the form¹³

$$L_{\text{meson}}[\vec{\pi}_{\text{cl}}] + L_{\text{Yukawa}}[\vec{\pi}_{\text{cl}}] = -M_{\text{cl}} + \frac{1}{2}M_{\text{cl}}\dot{\mathbf{X}}^2 + \mathcal{I}_{\text{cl}}\text{Tr}\dot{A}^\dagger\dot{A} + \dots. \quad (3.5)$$

¹³ The third term on the right-hand side, taken together with the identity (2.4), establishes for *all* leading-order baryon self-energy and baryon-meson vertex corrections, and for *any* value of the pion mass, the self-consistency of the hyperfine baryon mass splittings originally noted by Jenkins for the simplest such graph in the chiral limit [27]. As for the first two terms on the right-hand side, the fact that the same M_{cl} appears twice, with a relative weighting of $-\frac{1}{2}\dot{\mathbf{X}}^2$, follows trivially

Since $\vec{\pi}_{\text{cl}} \sim \sqrt{N_c}$ it follows that M_{cl} and \mathcal{I}_{cl} scale like N_c , just like M_{bare} and $\mathcal{I}_{\text{bare}}$. The dots in Eq. (3.5) indicate terms suppressed in the $1/N_c$ expansion, such as $\dot{\mathbf{X}}\dot{A}$ cross terms.¹⁴

The lesson of Eq. (3.5) is that the classical meson cloud $\vec{\pi}_{\text{cl}}$ (likewise $\vec{\rho}_{\text{cl}}$, ω_{cl} , σ_{cl} , etc.) gives a *form-preserving* and *leading-order*¹⁵ correction to the ‘bare’ baryon expressions (2.3)-(2.5), so that effectively

$$M_{\text{bare}}^J \longrightarrow M_{\text{ren}}^J = M_{\text{ren}} + \frac{J(J+1)}{2\mathcal{I}_{\text{ren}}} \quad (3.6)$$

where the renormalized baryon mass and moment of inertia are simply the sums¹⁶

$$M_{\text{ren}} = M_{\text{bare}} + M_{\text{cl}} , \quad \mathcal{I}_{\text{ren}} = \mathcal{I}_{\text{bare}} + \mathcal{I}_{\text{cl}} . \quad (3.7)$$

3.3. Hedgehog meson clouds

We now examine more carefully the structure of the classical meson cloud. Once again a helpful example is the “pions-only” Lagrangian (3.1). A simpler recasting of the Euler-Lagrange equation (3.2) comes from nailing the baryon’s center of mass at the origin and its (iso)spin orientation at the North pole, $\mathbf{X}(t) = 0$ and $A(t) = 1$, in which case (3.2) becomes [9]

$$(-\nabla^2 + m_\pi^2)\pi_{\text{stat}}^a(\mathbf{x}) + \frac{\partial V}{\partial \pi_{\text{stat}}^a} = 3g_{\pi NN}^{\text{bare}} \frac{\partial}{\partial x^a} \delta^3(\mathbf{x}) . \quad (3.8)$$

from Lorentz invariance (as Jim Hughes has reminded us). So long as the Lagrangian *density* is a Lorentz scalar, meaning that $\mathcal{L}(x) \rightarrow \mathcal{L}(x')$ as $x \rightarrow x'$, then $L(t) \equiv \int d^3\mathbf{x} \mathcal{L}(x) \rightarrow \int d^3\mathbf{x} \mathcal{L}(x') = \sqrt{1 - \dot{\mathbf{X}}^2} L(t') = (1 - \frac{1}{2}\dot{\mathbf{X}}^2 + \mathcal{O}(\dot{\mathbf{X}}^4))L(t')$, where $\sqrt{1 - \dot{\mathbf{X}}^2}$ is the change-of-frames Jacobian. One *cannot* ignore the Lorentz contraction of the cloud, as the two masses would then be unequal.

¹⁴ To prove that such terms are suppressed one needs to anticipate the findings of Sec. 3.3 below, and check that when the classical meson fields are precisely hedgehogs the cross terms vanish by symmetry upon spatial integration. They are only nonvanishing to the extent that the cloud deviates from the hedgehog ansatz, which it does at a higher order in $1/N_c$ [6,35].

¹⁵ This contrasts with the quantum corrections to the mass of the Skyrmion, which are only $\mathcal{O}(N_c^0)$. This is because the Skyrmion, unlike the “bare” nucleon, is the solution to an Euler-Lagrange equation.

¹⁶ The reader might be confused about the present definition of mass renormalization, versus the use of a conventional mass counterterm $\delta M = M_{\text{bare}} - M_{\text{ren}}$. In fact, they are the same thing. By definition, δM must be tuned to cancel the shift in the pole of the propagator away from M_{ren} induced by the interactions with the mesons. Since the nonrelativistic propagator $i/(k_0 - M + i\epsilon)$ Fourier transforms to $\theta(\Delta t)e^{-iM\Delta t}$, this simply means that $-i\delta M\Delta t$ must cancel the meson cloud contribution $-iM_{\text{cl}}\Delta t$ to the effective action. But this condition $\delta M = -M_{\text{cl}}$ is just a rewrite of Eq. (3.7), *QED*.

The solution is termed the “static pion cloud” $\vec{\pi}_{\text{stat}}(\mathbf{x})$, whereupon $\vec{\pi}_{\text{cl}}$ is approximated by

$$\pi_{\text{cl}}^a(\mathbf{x}, t) \cong D_{al}^{(1)}(A(t'))\pi_{\text{stat}}^l(\mathbf{x}') \quad (3.9)$$

up to $1/N_c$ corrections, the primes denoting the baryon’s center-of-mass frame as always. So it will suffice to focus on Eq. (3.8) rather than the more complicated time-dependent equation (3.2). In terms of $\vec{\pi}_{\text{stat}}$, the quantities M_{cl} and \mathcal{I}_{cl} are explicitly given by

$$M_{\text{cl}} = \int d^3\mathbf{x} \left[\frac{1}{2}(\partial_i \vec{\pi}_{\text{stat}})^2 + \frac{1}{2}m_\pi^2 \vec{\pi}_{\text{stat}}^2 + V(\vec{\pi}_{\text{stat}}) - 3g_{\pi NN}^{\text{bare}} \vec{\pi}_{\text{stat}} \cdot \nabla \delta^3(\mathbf{x}) \right] \quad (3.10)$$

and

$$\mathcal{I}_{\text{cl}} = \frac{2}{3} \int d^3\mathbf{x} \vec{\pi}_{\text{stat}}^2 . \quad (3.11)$$

What does $\vec{\pi}_{\text{stat}}$ look like? An important hint is that the index ‘ a ’ lives in *isospace* on the left-hand side and ordinary space on the right-hand side of Eq. (3.8). Therefore, as in the Skyrme model, the solution can generically be found in the maximally symmetric “hedgehog ansatz,” which equates these two spaces [9]:

$$\vec{\pi}_{\text{stat}}(\mathbf{x}) = \frac{f_\pi}{2} \hat{\mathbf{x}} F(r) \quad (3.12)$$

where $r = |\mathbf{x}|$ and $\hat{\mathbf{x}} = \mathbf{x}/r$. In turn, the cloud profile $F(r)$ solves a model-dependent nonlinear ordinary differential equation in the radial coordinate r , obtained by plugging (3.12) into (3.8).

Even if additional mesons are incorporated as per Eq. (2.11), the coupled static equations (one for each meson species) are still solved in the hedgehog ansatz, suitably generalized in the manner familiar from vector-meson-augmented Skyrme models [31,36]:

$$\begin{aligned} \rho_{\text{stat}}^{ai}(\mathbf{x}) &= f_\pi \epsilon_{iak} \hat{x}^k G(r) , & \rho_{\text{stat}}^{a0}(\mathbf{x}) &= 0 , & \sigma_{\text{stat}}(\mathbf{x}) &= f_\pi H(r) , \\ \omega_{\text{stat}}^i(\mathbf{x}) &= 0 , & \omega_{\text{stat}}^0(\mathbf{x}) &= f_\pi K(r) , & \text{etc.} , \end{aligned} \quad (3.13)$$

where ‘ i ’ and ‘ a ’ label spin and isospin, respectively. Since $f_\pi \sim \sqrt{N_c}$ has been factored out explicitly, the profiles F , G , H and K each scale like N_c^0 . In general they obey model-dependent coupled nonlinear radial ODE’s.

3.4. Ultraviolet divergences and the large- N_c renormalization group

The above discussion contains something of a cheat: as written, Eq. (3.8) only admits a mathematically well-defined solution in the free-pion case $V(\vec{\pi}) \equiv 0$, in which case obviously

$$\vec{\pi}_{\text{stat}}(\mathbf{x}) \propto \vec{\nabla} \frac{e^{-m_\pi r}}{r}. \quad (3.14)$$

For nonvanishing V , the lack of a solution to this nonlinear equation is due to the exact pointlike nature of the δ -function source.¹⁷ So, too, the cloud parameters M_{cl} and \mathcal{I}_{cl} introduced in Eq. (3.5) are actually ill-defined, diverging in the ultraviolet. An ultraviolet cutoff is required. This should come as no surprise: in most hadron models the need for such a cutoff arises as early in the discussion as the first loop correction in the original Feynman graphs (e.g., Figs. 2b-c). But even if one were to concoct a meson model free of this type of divergence at the level of the original graphs, a cutoff $\Lambda \sim N_c^0$ on the meson momenta would *still* be required for the self-consistency of the subsequent formalism; specifically, one needs to ensure that the baryon always stays in the vicinity of its rest frame even after an arbitrary number of interactions with the mesons. In fact, if instead one were to permit meson momenta of order N_c , in particular above the $N\bar{N}$ threshold, it is plausible that the entire effective Lagrangian approach breaks down (see Ref. [8], Sec. 8.3).

The simplest fix, with interesting consequences as we shall see, is to smear out the δ -function in some manner,

$$\delta^3(\mathbf{x}) \longrightarrow \delta_\Lambda^3(\mathbf{x}), \quad (3.15)$$

over a length scale Λ^{-1} . While details of this regulator should not matter for sufficiently large Λ , we will nevertheless insist that $\delta_\Lambda^3(\mathbf{x})$ be spherically symmetric, so that the hedgehog ansatz remains valid even for finite Λ , an enormous technical simplification.

Now suitably regulated, Eq. (3.8) (returning to the pions-only example) is easily solved numerically for $F(r)$. The solution is shown schematically in Fig. 8. For r well inside the classical cloud, whose radius is determined by the parameters of V , the behavior of $F(r)$ is highly model-dependent. But for $r \gg m_\pi^{-1}$, Eq. (3.8) linearizes, and one finds

$$F(r) \longrightarrow \frac{3g_{\pi NN}^{\text{ren}}}{2\pi f_\pi} \left(\frac{1}{r^2} + \frac{m_\pi}{r} \right) e^{-m_\pi r} \quad (3.16)$$

¹⁷ This arcane technical point about the lack of a well-defined solution is confirmed in the explicit examples of Secs. 5-8 below, as the reader can verify by imagining the following exercise. Hold $g_{\pi NN}^{\text{bare}}$ fixed (instead of $g_{\pi NN}^{\text{ren}}$ as in the large- N_c renormalization group) while taking the ultraviolet cutoff $\Lambda \rightarrow \infty$, and confirm that in so doing $\vec{\pi}_{\text{stat}}$ has either a singular limit, or no limit at all.

which follows from (3.12) and (3.14). Notice the new parameter, $g_{\pi NN}^{\text{ren}}$, which measures the height of the exponential tail. While its precise numerical value depends sensitively on the choices of $V(\vec{\pi})$ and Λ , its physical interpretation as the renormalized pion-nucleon pseudovector coupling constant is pleasingly model-independent. To our knowledge this identification was first made in Sec. 4 of Adkins, Nappi and Witten [2], and has recently been confirmed in Ref. [6] with a careful analysis of the LSZ amputation procedure.¹⁸ The behavior (3.16) is equally valid in the chiral limit:

$$F(r) \longrightarrow \frac{3g_{\pi NN}^{\text{ren}}}{2\pi f_\pi r^2} \quad (\text{massless pions}) . \quad (3.17)$$

In summary, for any given choice of meson Lagrangian, we have described an explicit numerical procedure—Eqs. (3.7) and (3.16)—for extracting the physical, renormalized parameters M_{ren} , \mathcal{I}_{ren} and $g_{\pi NN}^{\text{ren}}$ as functions of the Lagrangian input quantities M_{bare} , $\mathcal{I}_{\text{bare}}$, $g_{\pi NN}^{\text{bare}}$ as well as the UV cutoff Λ . Alternatively, one might wish to *fix* M_{ren} , \mathcal{I}_{ren} and $g_{\pi NN}^{\text{ren}}$, say to their experimental values

$$M_{\text{ren}} + \frac{3}{8\mathcal{I}_{\text{ren}}} \equiv M_N \cong 939 \text{ MeV} , \quad (3.18a)$$

$$M_{\text{ren}} + \frac{15}{8\mathcal{I}_{\text{ren}}} \equiv M_\Delta \cong 1232 \text{ MeV} , \quad (3.18b)$$

$$g_{\pi NN}^{\text{ren}} \cong \frac{13.5}{2M_N} , \quad (3.18c)$$

then solve implicitly for $M_{\text{bare}}(\Lambda)$, $\mathcal{I}_{\text{bare}}(\Lambda)$ and $g_{\pi NN}^{\text{bare}}(\Lambda)$. This latter approach seems the most reasonable to us, and will be our philosophy from now on. We call this novel program the *large- N_c renormalization group*, and devote the remainder of this paper to exploring its solutions in a variety of illustrative models.

¹⁸ While both these references discuss this particular issue in the context of the Skyrme model, the reader can verify that the conclusions are equally valid for effective Lagrangian models such as concern us here, with explicit baryon sources. It should come as no surprise that the LSZ residue is sensitive only to the asymptotic behavior (3.16), as this is a well-known property of Fourier transforms. The fact that the renormalized coupling is still pseudovector, like the bare coupling, is simply because the Fourier transform of a hedgehog is necessarily proportional to \mathbf{q} . The only subtle feature is this [6]: the existence of an LSZ pole precisely on the pion mass shell depends crucially on a small quadrupole [35] deviation of the Skyrme (or, in the present context, meson cloud) *away* from the hedgehog ansatz, induced by the baryon's (iso)rotations. This distortion is one of the $1/N_c$ corrections dropped in Eq. (3.9), as it is tangential to our present purposes.

4. Free pion Lagrangian and its continuum limit

Our first example consists simply of free massless pions,

$$\mathcal{L}_{\text{meson}} = \frac{1}{2}(\partial_\mu \vec{\pi})^2, \quad (4.1)$$

coupled derivatively to the $I = J$ baryon tower as per Eq. (2.8). In the hedgehog ansatz (3.12), the static Euler-Lagrange equation (3.8) becomes

$$F'' + \frac{2}{r}F' - \frac{2}{r^2}F = 6f_\pi^{-1}g_{\pi NN}^{\text{bare}}(\Lambda)\frac{\partial}{\partial r}\delta_\Lambda(r). \quad (4.2)$$

This being a linear equation, it is trivially solved using the method of Green's functions:

$$F(r) = 6f_\pi^{-1}g_{\pi NN}^{\text{bare}}(\Lambda)\int_0^\infty dr' r'^2 G(r, r')\frac{\partial}{\partial r'}\delta_\Lambda(r'), \quad (4.3)$$

where the massless Green's function that is well behaved at both $r = 0$ and $r = \infty$ is

$$G(r, r') = -\frac{r_{<}}{3r_{>}^2}, \quad r_{<} = \min\{r, r'\}, \quad r_{>} = \max\{r, r'\}. \quad (4.4)$$

The renormalized Yukawa coupling $g_{\pi NN}^{\text{ren}}$ is extracted from the large-distance behavior of F as per Eq. (3.17). With the mild (and relaxable) assumption that $\delta_\Lambda(r')$ has compact support, Eqs. (4.3) and (4.4) imply

$$F(r) \xrightarrow{r \rightarrow \infty} \frac{6g_{\pi NN}^{\text{bare}}(\Lambda)}{f_\pi r^2} \int_0^\infty dr' r'^2 \delta_\Lambda(r') = \frac{3g_{\pi NN}^{\text{bare}}(\Lambda)}{2\pi f_\pi r^2}. \quad (4.5)$$

We have made use of an integration by part, plus the requirement that the volume of δ_Λ be normalized to unity (regardless of other details of this smearing function). Comparing Eqs. (4.5) and (3.17), we deduce

$$g_{\pi NN}^{\text{bare}}(\Lambda) = g_{\pi NN}^{\text{ren}} \quad (4.6)$$

for all Λ , admittedly not a surprising result for free field theory, but a reassuring sanity check on our formalism.

This lack of any flow is consistent with what might be termed an “exact” Cheshire cat picture [15,13] (recalling the discussion in Sec. 1). In truth, this is the *only* model we have found where this perfect equality holds. For example, the mildest conceivable modification

to the Lagrangian (4.1) is to add a pion mass term. In that case the Green's function is, instead,

$$G(r, r') = \frac{1}{2m_\pi^3} \left[\left(\frac{1}{r_{<}^2} - \frac{m_\pi}{r_{<}} \right) e^{m_\pi r_{<}} - \left(\frac{1}{r_{<}^2} + \frac{m_\pi}{r_{<}} \right) e^{-m_\pi r_{<}} \right] \left(\frac{1}{r_{>}^2} + \frac{m_\pi}{r_{>}} \right) e^{-m_\pi r_{>}} \quad (4.7)$$

which properly reduces to (4.4) as $m_\pi \rightarrow 0$, and (4.6) is amended slightly to

$$g_{\pi NN}^{\text{bare}}(\Lambda) = \left(1 + \mathcal{O}(m_\pi^2/\Lambda^2) \right) g_{\pi NN}^{\text{ren}} . \quad (4.8)$$

In either variation, massless or massive, the continuum limit $\Lambda \rightarrow \infty$ can be safely taken, and the ‘‘ultraviolet fixed point’’ that emerges is just what one started with: a theory of free pions derivatively coupled to the baryon tower. This is entirely expected, since as mentioned earlier $V(\vec{\pi}) \equiv 0$ is the only case in which Eq. (3.8) as written already has a *bona fide* solution, namely, Eq. (3.14), and there is no actual need to smear out the δ -function source. We now turn to more interesting examples where these statements no longer hold, and where the breakdown of the ‘‘exact’’ Cheshire cat picture is much more severe than Eq. (4.8).

5. The nonlinear σ model and its *lack of continuum limit*

For our second example, consider the nonlinear σ model for pions,

$$\mathcal{L}_{\text{meson}} = \frac{f_\pi^2}{16} \text{Tr} \partial_\mu U^\dagger \partial^\mu U , \quad U = \exp(2i\vec{\pi} \cdot \vec{\tau}/f_\pi) , \quad (5.1)$$

again augmented by the bare Yukawa coupling (2.8). The static Euler-Lagrange equation (3.8) now works out to

$$F'' + \frac{2}{r} F' - \frac{1}{r^2} \sin 2F = 6f_\pi^{-1} g_{\pi NN}^{\text{bare}}(\Lambda) \frac{\partial}{\partial r} \delta_\Lambda(r) . \quad (5.2)$$

Solving this nonlinear equation for $F(r)$ requires that we specify a smearing of the source. For convenience, we follow Ref. [17], and choose a radial step-function

$$\delta_\Lambda(r) = \begin{cases} \frac{3\Lambda^3}{4\pi} & : \quad r \leq \Lambda^{-1} \\ 0 & : \quad r > \Lambda^{-1} \end{cases} \quad (5.3)$$

which is properly normalized to unit volume. The technical advantage, which we exploit presently, is that the right-hand side of Eq. (5.2) is now proportional to a *true* δ -function, since

$$\frac{\partial}{\partial r} \delta_\Lambda(r) = -\frac{3\Lambda^3}{4\pi} \delta(r - \Lambda^{-1}) . \quad (5.4)$$

There is also a conceptual advantage: the right-hand side of (5.4) means that the baryon and meson degrees of freedom only interact at the “bag radius” Λ^{-1} , which sharpens the analogy to the traditional chiral bag [10–13].

With this convenient choice of regulator, the prescription for satisfying Eq. (5.2) is transparent: First solve the *homogeneous* version of Eq. (5.2), namely

$$F'' + \frac{2}{r}F' - \frac{1}{r^2}\sin 2F = 0, \quad (5.5)$$

for $r < \Lambda^{-1}$ (“region I”) and for $r > \Lambda^{-1}$ (“region II”) subject to the boundary condition (3.17); next, match the solutions in these two regions, $F_I(r)$ and $F_{II}(r)$, at the point $r = \Lambda^{-1}$; and finally, read off $g_{\pi NN}^{\text{bare}}(\Lambda)$ from the slope discontinuity,

$$g_{\pi NN}^{\text{bare}}(\Lambda) = \frac{2}{9}\pi f_\pi \Lambda^{-3} (F'_I(\Lambda^{-1}) - F'_{II}(\Lambda^{-1})). \quad (5.6)$$

This 3-step graphical procedure is illustrated in Fig. 9. The curves $F_{II}(r)$ and $F_I(r)$ are displayed in Figs. 9a and 9b, respectively. The curve $F_{II}(r)$ is uniquely specified by $g_{\pi NN}^{\text{ren}}$ through the asymptotic formula (3.17). In contrast, $F_I(r)$ actually stands for an entire one-parameter family of curves related by dilatations, $F_I(r) \rightarrow F_I(\lambda r)$, thanks to the scale invariance of Eq. (5.5). For any specified value of the cutoff Λ , the scale parameter λ needs to be tuned so that $F_I(\Lambda^{-1}) = F_{II}(\Lambda^{-1})$. Note that F_I , unlike F_{II} , attains a maximum value $F_I^{\text{max}} \cong .58\pi$ before dropping back down towards $\pi/2$.

Let us discuss the qualitative behavior of the large- N_c renormalization group as the cutoff increases from zero. In the infrared regime $\Lambda \ll (f_\pi/g_{\pi NN}^{\text{ren}})^{1/2}$, the flow of $g_{\pi NN}^{\text{bare}}(\Lambda)$ necessarily approaches the free massless pion case, Eq. (4.6). This is simply because the patched-together profile $F(r)$ is small everywhere, in which case Eq. (5.2) reduces to Eq. (4.2) up to $\mathcal{O}(F^3)$ corrections. This is precisely the regime studied recently by Manohar [17], who correctly reproduced the $\mathcal{O}(m_\pi^3)$ non-analytic correction to the baryon mass familiar from one-loop chiral perturbation theory.

But the behavior of the renormalization group for higher Λ quickly diverges from the free-pions example. Notice that as Λ passes a first critical value Λ_1 (the point where $F_{II}(\Lambda_1^{-1}) = \pi/2$) a second disconnected solution to Eq. (5.2) emerges, in which F_{II} intersects F_I , not in the branch of the curve labeled “Region A” but rather in “Region B.” The flow in this branch is still dictated by Eq. (5.6), but since for any given Λ the value of $F'_I(\Lambda^{-1})$ differs between the two branches, the solutions are distinct. As Λ increases further, these two branches of $g_{\pi NN}^{\text{bare}}(\Lambda)$ gradually approach one another, until at a new critical value Λ_2 ,

defined by $F_{\text{II}}(\Lambda_2^{-1}) = F_1^{\text{max}}$, they coalesce. This latter scale is indicated by a cross in Fig. 9. From Fig. 9a one reads off $\Lambda_1^{-1} \cong .75(3g_{\pi NN}^{\text{ren}}/2\pi f_\pi)^{1/2}$ and $\Lambda_2^{-1} \cong .68(3g_{\pi NN}^{\text{ren}}/2\pi f_\pi)^{1/2}$, or in conventional units,

$$\Lambda_1 \cong 310 \text{ MeV} , \quad \Lambda_2 \cong 340 \text{ MeV} \quad (5.7)$$

using the physical values (3.18). We calculate $g_{\pi NN}^{\text{bare}}(\Lambda_2) \cong .43g_{\pi NN}^{\text{ren}}$. Crucially, for $\Lambda > \Lambda_2$, if one insists that $F_1(0) = 0$, then there is no way to match F_1 with F_{II} , hence no solution to Eq. (5.2).¹⁹

Thus we have exhibited two “phases” of the model (for want of a better term), the first being defined for $\Lambda \in [0, \Lambda_2]$, and the second only for $\Lambda \in [\Lambda_1, \Lambda_2]$. The critical “bag radius” $\Lambda_2^{-1} \cong .6 \text{ fm}$ is the UV scale beyond which the “chiral bag” cannot be formed from the 2-derivative pion action (5.1) alone; higher-derivative terms must be added. Evidently this breakdown owes nothing to soft-pion arguments as one is accustomed to—but follows solely from large- N_c reasoning.

To be honest, for $\Lambda > \Lambda_2$, one *can* patch together a solution—if one allows the cloud to have nonzero winding number (*cf.* Eq. (6.5a) below). For example, there are four “phases” of the model with winding number unity, which are constructed as follows. Leave $F_{\text{II}}(r)$ the same as above, but let $F_1(r) \rightarrow F_1(r) + \pi$, exploiting a discrete symmetry of Eq. (5.2). There are two such solutions, again depending on whether the intersection takes place in “Region A” or in “Region B.” The two remaining solutions are generated, instead, by the discrete symmetry $F_1(r) \rightarrow -F_1(r) + \pi$. Likewise there are four phases of the model for any positive winding number n , generated by²⁰ $F_1(r) \rightarrow \pm F_1(r) + n\pi$. Each such phase exists only for a finite interval in the cutoff Λ . In particular—unlike the free-pions example—here there is no phase within which one can take the continuum limit $\Lambda \rightarrow \infty$. In other words, *this model lacks an ultraviolet fixed point.*

Of course, there is no reason whatsoever that an effective field theory need have a continuum limit. It would be perfectly reasonable to fix Λ at a finite value less than Λ_2

¹⁹ Technically speaking, the two independent branches of $g_{\pi NN}^{\text{bare}}(\Lambda)$, which have coalesced at Λ_2 , leave the real axis and bifurcate into complex conjugate pairs for $\Lambda > \Lambda_2$.

²⁰ We suspect that these higher winding-number clouds may be, like the hedgehog Skyrminion in the $B = 2$ sector [1,37], unstable to small deformations in the cloud *away* from the hedgehog ansatz, but we have not looked for any such deformations, neither in the present model nor in the ones to follow.

where the “chiral bag” still makes sense, and to calculate, for example, the static properties of this hybrid nucleon, *à la* Adkins, Nappi and Witten [2]. Nevertheless, it is instructive to pose the question: In a generic theory, if the continuum limit can in fact be taken, what type of UV fixed point might one expect? In the free-meson examples of Sec. 4, $g_{\pi NN}^{\text{bare}}(\Lambda)$ runs to a finite, nonzero value as $\Lambda \rightarrow \infty$. But this behavior must be the exception rather than the rule. For, a nonzero limiting value of $g_{\pi NN}^{\text{bare}}(\Lambda)$ suggests that a solution to Eq. (3.8) exists even for a non-vanishing right-hand side with an exact δ -function source. Except for the free-meson case $V \equiv 0$, we have yet to discover a differential equation where this is possible. Instead, it is far more plausible that $g_{\pi NN}^{\text{bare}}(\Lambda)$ is the coupling constant of an “irrelevant operator,” and *vanishes* in the ultraviolet (as suggested by the factor of Λ^{-3} on the right-hand side of Eq. (5.6)). The resulting continuum theory would then be completely independent of the baryonic degrees of freedom, an interesting example of “universality” [4]. In this event, Eq. (3.8) admits a solution if (and only if?) the meson Lagrangian supports a nontrivial configuration in the absence of a baryonic source—meaning a soliton or Skyrmion, either topological or energetic.

Viewed in this light, it is no surprise that the nonlinear σ model coupled to the baryon tower has no UV limit, as we have just learned. Plausibly, this is because Eq. (5.1) does not by itself support a Skyrmion. The reason is Derrick’s famous “no go” theorem (a variant of the virial theorem) [18]: if one posits a static Euler-Lagrange solution $U_{\text{stat}}(\mathbf{x})$, then the energy functional

$$E[U_{\text{stat}}] = \frac{f_\pi^2}{16} \int d^D \mathbf{x} \text{Tr} \partial_i U_{\text{stat}}^\dagger \partial_i U_{\text{stat}} , \quad (5.8)$$

rather than being stationary, can actually be lowered arbitrarily by a homogeneous rescaling

$$U_{\text{stat}}(\mathbf{x}) \longrightarrow U_{\text{stat}}(\lambda \mathbf{x}) , \quad E[U_{\text{stat}}] \longrightarrow \frac{1}{\lambda^{D-2}} E[U_{\text{stat}}] ; \quad (5.9)$$

therefore, no such solution can exist.²¹ There are several known ways to modify the nonlinear σ model to prevent such a “Derrick collapse.” One way, which we examine in the following Section, is simply to reduce the dimensionality of space from $D = 3$ to the “critical dimension” $D = 2$, as Eq. (5.9) suggests. As a bonus, the resulting toy model turns out to be analytically soluble. Alternatively, and more physically, in Secs. 7 and 8 we will augment the Lagrangian (5.1) by the 4-derivative “Skyrme term,” and explore the interesting, and unexpected, consequences.

²¹ This point was apparently missed by Gervais and Sakita [14], whose Eqs. (5.19)-(5.20) admit no solution.

6. An exactly soluble 2+1 dimensional model with a nontrivial UV fixed point

Motivated by the above discussion, we would like to construct a 2+1 dimensional model which parallels as closely as possible the nonlinear σ model of the previous Section. To make the analogy as plain as possible, it is helpful to recall an alternate parametrization of the pion field to that given in Eq. (5.1). Rather than $U = \exp(2i\vec{\pi} \cdot \vec{\tau}/f_\pi)$, take

$$U = u_0 + i\mathbf{u} \cdot \vec{\tau}, \quad u_0 + \mathbf{u}^2 = 1, \quad \vec{\pi} = \frac{f_\pi}{2} \mathbf{u}, \quad (6.1)$$

in terms of which the nonlinear σ model Lagrangian (5.1) is simply

$$\mathcal{L}_{\text{meson}}^{3\text{D}} = \frac{f_\pi^2}{8} [(\partial_\mu u_0)^2 + (\partial_\mu u_1)^2 + (\partial_\mu u_2)^2 + (\partial_\mu u_3)^2]. \quad (6.2a)$$

The natural 2+1 dimensional analog is then²²

$$\mathcal{L}_{\text{meson}}^{2\text{D}} = \frac{f^2}{8} [(\partial_\mu n_0)^2 + (\partial_\mu n_1)^2 + (\partial_\mu n_2)^2], \quad n_0^2 + n_1^2 + n_2^2 = 1. \quad (6.2b)$$

Just as the choice of vacuum $(u_0, \mathbf{u}) = (1, \mathbf{0})$ spontaneously breaks the $O(4)$ chiral symmetry of (6.2a) down to isospin $O(3)$, so too the vacuum choice $(n_0, \mathbf{n}) = (1, 0, 0)$ in (6.2b) breaks “chiral” $O(3)$ down to “isospin” $O(2)$.

The hedgehog ansatz for the pion cloud,

$$(u_0, \mathbf{u}) = (\cos F(r), \hat{\mathbf{x}} \sin F(r)), \quad (6.3a)$$

will prove equally applicable to the lower-dimensional model,

$$(n_0, \mathbf{n}) = (\cos F(r), \hat{\mathbf{x}} \sin F(r)). \quad (6.3b)$$

Evaluated on these ansätze, the Hamiltonians are quite similar:

$$H_{3\text{D}}[F] = \frac{f_\pi^2}{8} \int d^3\mathbf{x} \left(F'^2 + 2 \frac{\sin^2 F}{r^2} \right) \quad (6.4a)$$

versus

$$H_{2\text{D}}[F] = \frac{f^2}{8} \int d^2\mathbf{x} \left(F'^2 + \frac{\sin^2 F}{r^2} \right), \quad (6.4b)$$

²² The mesonic sector of this toy model is a simplified version of the “baby Skyrme model” of Ref. [38].

respectively. But there is a major difference in the winding number formulae between the two models:²³

$$W_{3D}[F] = - \int d^3\mathbf{x} \frac{F' \sin^2 F}{2\pi^2 r^2} = \frac{1}{\pi} [F(0) - F(\infty)] \quad (6.5a)$$

versus

$$W_{2D}[F] = - \int d^2\mathbf{x} \frac{F' \sin F}{4\pi r} = -\frac{1}{2} [\cos F(0) - \cos F(\infty)] . \quad (6.5b)$$

In other words, whereas in three spatial dimensions the hedgehog ansatz is broad enough to encompass all integer winding numbers, the same is *not* true in two dimensions where winding number is restricted to the three values $\{-1, 0, +1\}$ as follows from Eq. (6.5b).²⁴ This caveat is irrelevant for present purposes, and so we press on.

There is a well-known rewrite of the $O(3)$ model in terms of the “conformal variables” [39]

$$w = \frac{n_1 + in_2}{1 + n_0}, \quad \bar{w} = \frac{n_1 - in_2}{1 + n_0}. \quad (6.6)$$

These variables (canonically rescaled by a factor of $f/2$) are closer in spirit to the “old” pion representation (5.1), in that there are no extraneous fields such as u_0 or n_0 that need to be eliminated with a spherical constraint. Paralleling the previous Section, we will therefore use the w ’s, not the n ’s, in constructing the Yukawa coupling.

Next we turn to the baryons. The obvious “toy” analog of the $I = J$ tower is an infinite sequence of states $|\nu\rangle$ that transform as (ν, ν) , $\nu = \pm\frac{1}{2}, \pm\frac{3}{2}, \pm\frac{5}{2}, \dots$, under “isospin” $O(2) \cong U(1)$ and spatial $U(1)$ rotations in the x - y plane. A spin \times isospin invariant Yukawa coupling in the baryon rest frame then has the form

$$\frac{f}{2} \frac{\partial w}{\partial z} \sum_{\nu=\pm\frac{1}{2}, \pm\frac{3}{2}, \dots} g_\nu |\nu + 1\rangle \langle \nu| + \text{H.c.} \quad (6.7)$$

Here the g_ν are arbitrary complex constants, $z = x + iy$, and the operator $|\nu + 1\rangle \langle \nu|$ simply means that the difference of the $U(1)$ (iso)spin charges between the initial and final baryons must be unity.

²³ Winding number is given, respectively, by $W = -\frac{1}{24\pi^2} \int d^3\mathbf{x} \epsilon_{ijk} \text{Tr} T_i T_j T_k$ in three dimensions, where $T_i = U^\dagger \partial_i U$, and $W = \frac{1}{8\pi} \int d^2\mathbf{x} \epsilon_{\nu\mu} n \cdot \partial_\mu n \times \partial_\nu n$ in two dimensions, where n means (n_0, n_1, n_2) .

²⁴ A mild extension of the hedgehog ansatz (6.3b) covers the sectors with winding number n : rewrite $\hat{\mathbf{x}}$ as $(\cos \theta, \sin \theta)$ and replace this by $(\cos n\theta, \sin n\theta)$ instead.

An intelligent way to generate such a coupling is to work in the collective coordinate basis $|\theta\rangle$, $\theta \in U(1)$, analogous to $|A\rangle$ in 3+1 dimensions. The baryon Lagrangian analogous to (2.3) is

$$\mathcal{L}_{\text{baryon}}^{2D} = -M_{\text{bare}} + \frac{1}{2}M_{\text{bare}}\dot{\mathbf{X}}^2 + \frac{1}{2}\mathcal{I}_{\text{bare}}\dot{\theta}^2, \quad (6.8)$$

the last term representing free motion on the $U(1)$ manifold. Another of Schulman's path integral identities [32],

$$\int_{\theta(t_1)=\theta_1}^{\theta(t_2)=\theta_2} \mathcal{D}\theta(t) \exp i \int dt \left(-M_{\text{bare}} + \frac{1}{2}\mathcal{I}_{\text{bare}}\dot{\theta}^2 \right) = \sum_{\nu=\pm\frac{1}{2}, \pm\frac{3}{2}, \dots} \langle \theta_2 | \nu \rangle e^{-i(t_2-t_1)M_{\text{bare}}^\nu} \langle \nu | \theta_1 \rangle \quad (6.9)$$

with

$$M_{\text{bare}}^\nu = M_{\text{bare}} + \frac{\nu^2}{2\mathcal{I}_{\text{bare}}} \quad \text{and} \quad \langle \nu | \theta \rangle = e^{i\nu\theta}, \quad (6.10)$$

equates such motion with the propagation of an infinite tower of energy eigenstates $|\nu\rangle$, just like Eqs. (2.4)-(2.6) for $SU(2)$. The Yukawa coupling analogous to (2.8) is then

$$\frac{1}{2}g_{\text{bare}} f \frac{\partial w}{\partial z'} e^{-i\hat{\theta}(t')} \delta^2(\mathbf{x}') + \text{H.c.}, \quad (6.11)$$

the primed space-time variables referring to the center-of-mass frame of the moving baryon as in Sec. 2. Note that Eq. (6.11) is a *special case* of Eq. (6.7), with all the g_ν 's equated to a single underlying Yukawa constant g_{bare} (to see this, copy the steps in Eq. (2.10)). This feature too is just like the higher-dimensional example: recall the proportionality rule (\mathbf{v}) reviewed in Sec. 2.1, and embodied in the matrix elements (2.10).

We have assembled all the ingredients necessary to write down the classical Euler-Lagrange equation for the meson cloud. The solution, w_{cl} , automatically sums up all contributions to one-meson absorption or emission from the baryon source, to leading order in the semiclassical expansion. In solving for w_{cl} , it is convenient as always to boost from the Lab frame to the body-fixed frame of the translating, (iso)rotating, Lorentz-contracting baryon:

$$w_{\text{cl}}(\mathbf{x}, t) = e^{i\hat{\theta}(t')} w_{\text{stat}}(\mathbf{x}') . \quad (6.12)$$

In turn, the static meson cloud $w_{\text{stat}}(\mathbf{x})$ finds a solution in the hedgehog ansatz, composed from (6.3b) and (6.6):

$$w_{\text{stat}}(\mathbf{x}) = \frac{z}{r} \tan \frac{F(r)}{2}, \quad r = \sqrt{z\bar{z}} . \quad (6.13)$$

Finally, the profile $F(r)$ obeys

$$\begin{aligned} F'' + \frac{1}{r}F' - \frac{1}{2r^2}\sin 2F &= \frac{g_{\text{bare}}(\Lambda)}{f} \sec^2 \frac{F(r)}{2} \frac{\partial}{\partial r} \delta_\Lambda(r) \\ &= -\frac{\Lambda^2 g_{\text{bare}}(\Lambda)}{\pi f} \sec^2 \frac{F(\Lambda^{-1})}{2} \delta(r - \Lambda^{-1}) . \end{aligned} \quad (6.14)$$

This follows straightforwardly from (6.4b), (6.11) and (6.13), plus an obvious transcription of the δ -function regulator (5.3) to two dimensions.

After this long build-up, we remind the reader of the original motivation behind this toy model: by recasting the nonlinear σ model in two spatial dimensions, we have side-stepped Derrick’s theorem, and increased the likelihood of finding a nontrivial UV fixed point to the large- N_c renormalization group equations. We will verify this presently. But already our efforts have yielded a bonus: unlike Eq. (5.5), the homogeneous variant of Eq. (6.14), namely

$$F'' + \frac{1}{r}F' - \frac{1}{2r^2}\sin 2F = 0 , \quad (6.15)$$

can be solved analytically. Indeed, switching independent variables to $\log r$ transforms this into the sine-Gordon equation, the solutions to which are the “baby (anti)Skyrmions”²⁵

$$F(r) = 2 \text{Tan}^{-1} \mu_{\text{I}} r \quad \text{or} \quad \pi - 2 \text{Tan}^{-1} \mu_{\text{II}} r \quad (6.16)$$

where μ_{I} and μ_{II} are arbitrary scale constants.

Figure 10 displays the patched-together solution to Eq. (6.14). In region II ($r > \Lambda^{-1}$) we choose the solution that decays to zero, $F_{\text{II}}(r) = \pi - 2 \text{Tan}^{-1} \mu_{\text{II}} r$, and fix μ_{II} by normalizing the large- r falloff to $g_{\text{ren}}/(2\pi f r)$:

$$\mu_{\text{II}} = \frac{4\pi f}{g_{\text{ren}}} . \quad (6.17)$$

As before, g_{ren} is the renormalized Yukawa constant of the model.²⁶ Next, pick $F_{\text{I}}(r) = 2 \text{Tan}^{-1} \mu_{\text{I}} r$ in region I ($r < \Lambda^{-1}$). Matching F_{I} to F_{II} at $r = \Lambda^{-1}$ implies

$$\mu_{\text{I}} = \frac{\Lambda^2 g_{\text{ren}}}{4\pi f} . \quad (6.18)$$

²⁵ These (anti-) solitons in 2+1 dimensions are also the well-known $O(3)$ (anti-) instantons in two Euclidean dimensions [39].

²⁶ The “ N_c ” scalings are $g_{\text{ren}} \sim f \sim \sqrt{N_c}$ in analogy with the 3+1 dimensional case. Although in this model N_c is no longer identified with the number of colors, it still usefully parametrizes the semiclassical expansion. To get the factors of π etc. right in the definition of g_{ren} , it suffices to solve with a Green’s function (cf. Sec. 4) the linearized version of (6.14), $F'' + F'/r - F/r^2 = (g_{\text{ren}}/f)\delta'_\Lambda(r)$, appropriate to the weak-field regime $F \ll 1$. Alternatively, one can extract the LSZ residue of the meson-mass-shell pole as per Ref. [6].

The running of g_{bare} is instantly read off from the slope discontinuity in Eq. (6.14):

$$g_{\text{bare}}(\Lambda) = \frac{\pi f}{\Lambda^2} \cos^2 \frac{F(\Lambda^{-1})}{2} \left(F'_{\text{I}}(\Lambda^{-1}) - F'_{\text{II}}(\Lambda^{-1}) \right) = \frac{g_{\text{ren}}}{\left[1 + \left(\frac{\Lambda g_{\text{ren}}}{4\pi f} \right)^2 \right]^2}. \quad (6.19)$$

As anticipated, $g_{\text{bare}}(\Lambda)$ approaches g_{ren} in the infrared, while vanishing rapidly ($\sim \Lambda^{-4}$) in the ultraviolet.

Note that for any *finite* value of the cutoff, baryon number in this model is measured in the mundane way, by the fermion number operator. Furthermore, the winding number (6.5b) of the patched-together meson cloud is zero, since $F(0) = F(\infty) = 0$. But at infinite Λ the picture looks very different: the baryons have entirely decoupled from the mesons thanks to (6.19), while the envelope of the sequence of meson clouds with increasing Λ is obviously a soliton or Skyrmion with winding number *unity*, namely $F(r) \equiv F_{\text{II}}(r)$. In this sense, baryon number can be said to have *transmuted* to winding number at infinite Λ . And in sharp contrast to the previous Section, the UV fixed point of our toy “chiral bag” model exists and is nontrivial: a “baby Skyrmion” model.

As a more sophisticated alternative, one may choose to define baryon number density as the *sum* of the usual explicit fermion number density and the winding number density, which is more in the spirit of Refs. [11–12]. For small Λ , winding number density is negligible everywhere; the mundane definition is recaptured, and is entirely concentrated inside the bag, $r \leq \Lambda^{-1}$. But for large Λ the situation is reversed: explicit fermion number density is screened by negative winding number density inside the bag, and the bulk of the baryon number is carried, in the form of winding number, by the meson cloud outside the bag. In the strict continuum limit, the bag is gone altogether, and only winding number remains. This is a greatly simplified variant (with nonrelativistic nucleons, rather than spectrally-flowing valence and sea quarks) of the scenario put forward by Goldstone and Jaffe [12].

We now exit toyland, return to 3+1 dimensions, augment the nonlinear σ model (5.1) by the well-known “Skyrme term” to overcome Derrick’s theorem, and examine under what circumstances the statements of the preceding paragraph can, or cannot, be made.

7. The Skyrme Lagrangian, with the Adkins-Nappi-Witten value of $g_{\pi NN}^{\text{ren}}$

Finally, and most physically, we take for the pion piece of the action the massless Skyrme Lagrangian [1,2]:

$$\mathcal{L}_{\text{meson}} \equiv \mathcal{L}_{\text{skyrme}} = \frac{f_\pi^2}{16} \text{Tr} \partial_\mu U^\dagger \partial^\mu U + \frac{1}{32e_s^2} \text{Tr} [U^\dagger \partial_\mu U, U^\dagger \partial_\nu U]^2. \quad (7.1)$$

We continue to assume that the pions are coupled to the $I = J$ tower of explicit baryon fields through Eq. (2.8). Since the two terms in (7.1) scale oppositely under dilatations (5.9), Derrick’s theorem is avoided, and $\mathcal{L}_{\text{skyrme}}$ supports a soliton: the original hedgehog Skyrmion (Fig. 11). In their Skyrme-model treatment, Adkins, Nappi and Witten take $f_\pi = 129 \text{ MeV}$ (vs. 186 MeV experimentally) and $e_s = 5.45$ in order to fit the nucleon and Δ masses [2]. In the present *non*-Skyrme-model approach, with explicit nucleons and Feynman diagrams rather than topology, our above-stated philosophy suggests instead that we peg these parameters to their experimental values (although e_s is not very well determined by $\pi\pi$ scattering). However, since our present aims are formal rather than phenomenological, it is actually best to leave them unspecified. What we *do* care about are their N_c assignments:

$$f_\pi^2 \sim \frac{1}{e_s^2} \sim N_c. \quad (7.2)$$

Thus N_c/\hbar factors out of the action, which justifies our usual semiclassical manipulations.

Given that the Lagrangian (7.1), like the toy model (6.2b), supports a soliton, what might we guess about the large- N_c renormalization group? Reasoning by analogy with the preceding Section, we might expect $g_{\pi NN}^{\text{bare}}(\Lambda)$ to vanish in the continuum limit, with the Skyrmion emerging as the UV fixed point of the family of meson-baryon “chiral bag” models. *But this naive scenario cannot generally be right!*

To see why not, let us return to a discussion from Sec. 1.4, and think about what does—and does not—flow in our program. What flows are the bare baryon mass and hyperfine mass splitting parameters $M_{\text{bare}}(\Lambda)$ and $\mathcal{I}_{\text{bare}}(\Lambda)$, as well as the bare Yukawa couplings $g_{\pi NN}^{\text{bare}}(\Lambda)$, $g_{\rho NN}^{\text{bare}}(\Lambda)$, etc. What does *not* flow are the purely mesonic Lagrangian couplings (f_π and e_s in Eq. (7.1), f in Eq. (6.2b), and so forth; see Fig. 12 for a discussion), as well as the *renormalized* parameters M_{ren} , \mathcal{I}_{ren} , $g_{\pi NN}^{\text{ren}}$, etc. These latter quantities, then, are independent variables at our disposal in the effective Lagrangian approach—and remain so even at the supposed endpoint of the large- N_c renormalization group flow. Now contrast this to the Skyrmion approach. Assume that f_π and e_s have been specified once and for

all, and look again at the resulting Skyrmion, Fig. 11. Notice that $g_{\pi NN}^{\text{ren}}$, rather than being an additional tuneable parameter as we have just argued, is instead fixed by Eq. (3.17) in terms of these meson parameters, as originally shown by Adkins, Nappi and Witten [2]:

$$g_{\pi NN}^{\text{ren}} \equiv g_{\pi NN}^{\text{ANW}} \cong \frac{18.0}{e_S^2 f_\pi}. \quad (7.3)$$

The puzzle can now be stated very clearly: If the Skyrme model is in fact connected to an effective Lagrangian model by RG flow, then where, why and how has the supposedly tuneable Yukawa degree of freedom in the latter disappeared?²⁷

The complete resolution of this paradox is the topic of this Section and the next, and goes as follows. When $g_{\pi NN}^{\text{ren}}$ is tuned to $g_{\pi NN}^{\text{ANW}}$ precisely, then the Skyrme model does indeed emerge as the UV fixed point of the “chiral bag” models, just as in Sec. 6. But for *all other* choices of $g_{\pi NN}^{\text{ren}}$, the physics is closer to that of Sec. 5: the large- N_c renormalization group only makes sense up to a critical value of the cutoff Λ_{crit} , and admits no continuum limit—neither the Skyrme model nor anything else.

We now flesh this out explicitly. In the hedgehog ansatz (3.12), the Euler-Lagrange equation (3.8) implied by (7.1) reads

$$\begin{aligned} \left(1 + \frac{8 \sin^2 F}{e_S^2 f_\pi^2 r^2}\right) F'' + \frac{2}{r} F' - \frac{\sin 2F}{r^2} \left(1 + \frac{4 \sin^2 F}{e_S^2 f_\pi^2 r^2} - \frac{4F'^2}{e_S^2 f_\pi^2}\right) \\ = -\frac{9\Lambda^3 g_{\pi NN}^{\text{bare}}(\Lambda)}{2\pi f_\pi} \delta(r - \Lambda^{-1}). \end{aligned} \quad (7.4)$$

We have again adopted the regulator (5.3). As above, we construct solutions $F_I(r)$ and $F_{\text{II}}(r)$ to the homogeneous variant

$$\left(1 + \frac{8 \sin^2 F}{e_S^2 f_\pi^2 r^2}\right) F'' + \frac{2}{r} F' - \frac{\sin 2F}{r^2} \left(1 + \frac{4 \sin^2 F}{e_S^2 f_\pi^2 r^2} - \frac{4F'^2}{e_S^2 f_\pi^2}\right) = 0, \quad (7.5)$$

match them up at $r = \Lambda^{-1}$, and extract the running of $g_{\pi NN}^{\text{bare}}$ from the slope discontinuity:

$$g_{\pi NN}^{\text{bare}}(\Lambda) = \frac{2\pi f_\pi}{9\Lambda^3} \left(1 + \frac{8\Lambda^2 \sin^2 F(\Lambda^{-1})}{e_S^2 f_\pi^2}\right) \left(F_I'(\Lambda^{-1}) - F_{\text{II}}'(\Lambda^{-1})\right). \quad (7.6)$$

For the remainder of this Section, we focus on the “measure zero” case when $g_{\pi NN}^{\text{ren}}$ is pegged to its Adkins-Nappi-Witten value (7.3). In that event $F_{\text{II}}(r) \equiv F_{\text{skyrme}}(r)$, the

²⁷ This paradox never came up in the toy model of Sec. 6 because of *scale invariance*: the Skyrmion $\pi - 2 \text{Tan}^{-1}(4\pi fr/g_{\text{ren}})$ exists for any independently-chosen values of f and g_{ren} .

Skyrmion profile of Fig. 11. For $F_I(r)$, we take the family of solutions to Eq. (7.5) that start at the origin and have increasing slope as Λ itself is increased (Fig. 13).

We can now evaluate Eq. (7.6). For small r , the Skyrmion profile may be Taylor-expanded:

$$F_{\text{skyrme}}(r) = \pi - c_1 e_s f_\pi r + \mathcal{O}(e_s f_\pi r)^3. \quad (7.7)$$

Therefore, the first term in parentheses in (7.6) is $1 + 8c_1^2 + \mathcal{O}(\Lambda^{-2})$ in the ultraviolet, where the numerical slope c_1 may be read off Fig. 11. The second term in parentheses is dominated for large Λ by

$$F_I'(\Lambda^{-1}) \sim \frac{c_2 \Lambda^2}{e_s f_\pi}, \quad (7.8)$$

where c_2 is another numerical constant.²⁸ Combining these expressions then gives

$$g_{\pi NN}^{\text{bare}}(\Lambda) \stackrel{\Lambda \rightarrow \infty}{\propto} \frac{1}{e_s \Lambda}. \quad (7.9)$$

Thus, just as in the toy model, the baryons decouple from the pions in the ultraviolet limit, at which point ordinary baryon number $\sum_{i_z, s_z} (N^\dagger N + \Delta^\dagger \Delta + \dots)$ effectively transmutes into the winding number of the pion cloud, Eq. (6.5a), in the manner discussed at the end of Sec. 6.

8. The Skyrme Lagrangian, with an incorrect choice of $g_{\pi NN}^{\text{ren}}$

Finally, we analyze the “generic” case when $g_{\pi NN}^{\text{ren}}$ differs from its Skyrme-model value $g_{\pi NN}^{\text{ANW}}$. In what way is the solution to Eqs. (7.4)-(7.6) affected? Consider how, in practice, one constructs $F_{\text{II}}(r)$ numerically. One first sets $F_{\text{II}} \sim 3g_{\pi NN}^{\text{ren}}/(2\pi f_\pi r^2)$ in the asymptotic regime $r \gg (e_s f_\pi)^{-1}$, then integrates inwards towards the origin, and in so doing, encounters a surprise: rather than intercepting the y axis at π as in the previous case with $g_{\pi NN}^{\text{ren}} = g_{\pi NN}^{\text{ANW}}$, or diverging for small r as in the nonlinear σ model of Sec. 5, F_{II} invariably

²⁸ This Λ^2 behavior is surprising, since generically along curve I, $F_I'(r) \sim \Lambda$ instead, as is easily argued. However, very near the point where F_I crosses π , its slope changes over to a Λ^2 behavior. An interesting way of proving this statement (which we first observed numerically) is with the calculus of variations. Specifically, if one performs a small deformation of the cloud analogous to that shown in Fig. 15 below, and demands that the first variation vanish (as it must), one derives Eq. (7.8), including an explicit expression for c_2 in terms of c_1 and a definite integral of the Skyrme Hamiltonian.

hits the y axis at a *half*-integral multiple $(n + \frac{1}{2})\pi$, as shown in Fig. 14a. This behavior can be confirmed analytically. Linearizing Eq. (7.5) about such half-integral values forces

$$\begin{aligned}
F_{\text{II}}(r) &\xrightarrow{r \rightarrow 0} (n + \frac{1}{2})\pi + \text{const.} \times r^{(1+i\sqrt{3})/2} + \text{const.} \times r^{(1-i\sqrt{3})/2} \\
&\quad + \mathcal{O}(r^{3/2}) \\
&= (n + \frac{1}{2})\pi - (\mu_1 r)^{1/2} \cos\left(\frac{\sqrt{3}}{2} \log \mu_2 r\right) + \mathcal{O}(r^{3/2}).
\end{aligned} \tag{8.1}$$

The fact that there are two independent constants here, μ_1 and μ_2 , shows that this is indeed a generic family of solutions to Eq. (7.5).²⁹ The bizarre oscillatory behavior of this essential singularity is verified in Fig. 14b.

Of course, the family of F_I curves is still given by Fig. 13, and $g_{\pi NN}^{\text{bare}}(\Lambda)$ is again read off from the slope discontinuity (7.6) at $r = \Lambda^{-1}$, so one can still patch together a *bona fide* solution to Eq. (7.4). But, as always, this solution is only physically relevant if it is *locally stable* against small deformations of the meson cloud.

We have carefully investigated this issue of local stability (albeit only within the hedgehog ansatz), and identified one dangerous mode, described in Fig. 15. Since we are perturbing about an Euler-Lagrange solution, first variations necessarily vanish. Instead, our stability analysis focuses on the sign of the coefficient Q of quadratic variations in this mode, a positive (negative) value indicating (in)stability. We have calculated (see Appendix A for details):

$$Q \xrightarrow{\Lambda \rightarrow \infty} \text{const.} \times (e_s^{-3} f_\pi \Lambda)^{1/2} \cos\left(\frac{\sqrt{3}}{2} \log \mu_2 \Lambda^{-1}\right) + \mathcal{O}(\Lambda^0). \tag{8.2}$$

Therefore, for fixed $g_{\pi NN}^{\text{ren}} \neq g_{\pi NN}^{\text{ANW}}$, and sufficiently large Λ , the model exhibits alternating “phases” of local stability and instability along a large- N_c renormalization group trajectory.

²⁹ The only other self-consistent solutions at small r start at integer multiples of π , and are of the form $n\pi - \mu r + \mathcal{O}(r^3)$, e.g., the Skyrminion itself. Unlike Eq. (8.1), these are only *one*-parameter families (parametrized by μ), so one never “accidentally” stumbles upon them when numerically integrating inwards. Amusingly, the same phenomenon holds true at *large* r as well [40] (cf. Fig. 9b): there are generic two-parameter families asymptoting to $(n + \frac{1}{2})\pi$, and special one-parameter families (again, including the Skyrminion) terminating at $n\pi$. So the 3+1 dimensional Skyrminion is “special” both at $r = 0$ and at $r = \infty$, hence has no free parameters. Of course, finiteness of the energy requires integer, not half-integer, boundary conditions at both ends, which we enforce on our patched-together “chiral bags.”

Mathematically, this behavior is traceable to the short-distance essential singularities (8.1) in the solutions to Eq. (7.5). Each such phase lasts half a period of the sinusoidal oscillation, thus:

unstable phases :

$$\Lambda \in [\Lambda_{\text{crit}}, \kappa \Lambda_{\text{crit}}], \Lambda \in [\kappa^2 \Lambda_{\text{crit}}, \kappa^3 \Lambda_{\text{crit}}], \Lambda \in [\kappa^4 \Lambda_{\text{crit}}, \kappa^5 \Lambda_{\text{crit}}], \dots \quad (8.3a)$$

stable phases :

$$\Lambda \in [\kappa \Lambda_{\text{crit}}, \kappa^2 \Lambda_{\text{crit}}], \Lambda \in [\kappa^3 \Lambda_{\text{crit}}, \kappa^4 \Lambda_{\text{crit}}], \Lambda \in [\kappa^5 \Lambda_{\text{crit}}, \kappa^6 \Lambda_{\text{crit}}], \dots \quad (8.3b)$$

Here $\kappa = \exp(2\pi/\sqrt{3})$ is the constant whose logarithm equals half a period, and Λ_{crit} is defined as the first appearance of this instability as the large- N_c renormalization group is pushed into the ultraviolet. Λ_{crit} is analogous to the Landau pole in quantum electrodynamics: it is the scale beyond which one cannot push the cutoff while requiring that the theory be stable. Of course, the value of Λ_{crit} depends sensitively on $g_{\pi NN}^{\text{ren}}$; in general, the closer the latter is to $g_{\pi NN}^{\text{ANW}}$, the greater we expect Λ_{crit} to be. In this language, the results of the previous Section may be understood as the statement that $\Lambda_{\text{crit}} \rightarrow \infty$ (stability regained) as $g_{\pi NN}^{\text{ren}} \rightarrow g_{\pi NN}^{\text{ANW}}$.

As in the nonlinear σ model of Sec. 5, one can also patch together pion clouds with nonzero winding number, but each of these is again locally stable only for finite ranges in Λ (and potentially locally *unstable* against small deformations *away* from the hedgehog ansatz). While the nature of the mathematical obstruction is somewhat different, the conclusion here is the same as for Sec. 5: the Skyrme Lagrangian, coupled to the baryon tower, admits no continuum limit when $g_{\pi NN}^{\text{ren}}$ differs from its canonical Skyrme-model value $g_{\pi NN}^{\text{ANW}}$. In this interesting way the “large- N_c renormalization group as filter” idea is realized.

We thank Jim Friar, Jim Hughes, Alex Kovner, Aneesh Manohar and Dick Silbar for useful comments, and Jessica Binder for help with the artwork. MPM is indebted to the Swansea physics department for hospitality during the time that much of this work was carried out. This draft was posted on the occasion of ND’s 30th birthday.

Appendix A. Cloud collapse in the Skyrme example when $g_{\pi NN}^{\text{ren}} \neq g_{\pi NN}^{\text{ANW}}$.

Derivation of the local instability

The primary goal of this Appendix is to derive the oscillatory expression (8.2) for the Gaussian coefficient Q of the mode shown in Fig. 15. For this purpose, we need to

construct the total energy of the cloud, $H_{\text{tot}}[F]$, keeping only the terms of $\mathcal{O}(N_c)$. The usual Skyrme-model Hamiltonian density is the sum of the contributions from the 2-derivative and 4-derivative terms,

$$\begin{aligned} \mathcal{H}_{\text{skyrme}} &= \mathcal{H}_{2\text{-deriv}} + \mathcal{H}_{4\text{-deriv}} \\ &= \frac{f_\pi^2}{8} \left(F'^2 + 2 \frac{\sin^2 F}{r^2} \right) + \frac{1}{2e_S^2} \left(\frac{\sin^4 F}{r^4} + 2 \frac{F'^2 \sin^2 F}{r^2} \right). \end{aligned} \quad (\text{A.1})$$

H_{tot} is itself the sum of three distinct parts, the contributions from region I, region II, plus the negative-definite energy of the Yukawa interaction with the baryonic source:

$$H_{\text{tot}}[F] = H_{\text{I}}[F] + H_{\text{II}}[F] + H_{\text{Yukawa}}[F] \quad (\text{A.2})$$

where

$$H_{\text{I}}[F] = 4\pi \int_0^{\Lambda^{-1}} r^2 dr \mathcal{H}_{\text{skyrme}}, \quad H_{\text{II}}[F] = 4\pi \int_{\Lambda^{-1}}^{\infty} r^2 dr \mathcal{H}_{\text{skyrme}}, \quad (\text{A.3})$$

and

$$H_{\text{Yukawa}}[F] = -\frac{9}{2} f_\pi \Lambda g_{\pi NN}^{\text{bare}}(\Lambda) F(\Lambda^{-1}) \quad (\text{A.4})$$

The point-like form of the latter is due to our special choice of smearing, Eq. (5.3). The defining equation for F , Eq. (7.4), is precisely the Euler-Lagrange equation

$$\frac{\delta}{\delta F} H_{\text{tot}}[F] = 0. \quad (\text{A.5})$$

Suppose that $F(r)$ is a patched-together solution to Eq. (7.4), and consider the effect of the small deformation of Fig. 15 on each of the three parts in Eq. (A.2). As constructed, the deformation keeps the matching point at $r = \Lambda^{-1}$ always, but changes the value of F at this point from $F_{\text{I}}(\Lambda^{-1})$ to $F_{\text{I}}((1 - \eta)\Lambda^{-1})$. With this sign convention, a positive value of η lowers the patched-together cloud so that it is closer to the vacuum $F(r) \equiv 0$, whereas a negative value of η raises the curve so that it is closer to the Skyrme of Fig. 11. We will treat η as an infinitesimal parameter, and will find it fruitful to keep all terms through order η^3 . The effect on H_{Yukawa} is immediate:³⁰

$$H_{\text{Yukawa}} \longrightarrow -\frac{9}{2} f_\pi \Lambda g_{\pi NN}^{\text{bare}}(\Lambda) \left[F_{\text{I}} - \eta \Lambda^{-1} F'_{\text{I}} + \frac{1}{2!} \eta^2 \Lambda^{-2} F''_{\text{I}} - \frac{1}{3!} \eta^3 \Lambda^{-3} F'''_{\text{I}} + \mathcal{O}(\eta^4) \right]. \quad (\text{A.6})$$

³⁰ From now on, F_{I} is short for $F_{\text{I}}(\Lambda^{-1})$ and likewise for its derivatives. Note that this equation is a perturbative expansion in η , *not* in Λ^{-1} : generically along the solution curve in region I, $F'_{\text{I}}(r) \sim \mathcal{O}(\Lambda)$, $F''_{\text{I}}(r) \sim \mathcal{O}(\Lambda^2)$, $F'''_{\text{I}}(r) \sim \mathcal{O}(\Lambda^3)$, and so forth, so that the terms in brackets are each nominally $\mathcal{O}(\Lambda^0)$. (Two important exceptions to this generic behavior along curve I: when $F_{\text{I}}(r)$ is near π then $F'_{\text{I}}(r) \sim \Lambda^2$ rather than Λ as explained earlier, and also, when $F_{\text{I}}(r)$ is near $\pi/2$ then $F''_{\text{I}}(r) \sim \Lambda^{3/2}$ rather than Λ^2 as implied by Eq. (A.7).) Another possibly confusing point: $g_{\pi NN}^{\text{bare}}(\Lambda)$ does *not* vary under this deformation; it is just a Lagrangian parameter like any other for the purposes of the variational calculus.

Next, we examine H_I . By design, $F_I(r)$ is supposed to remain a solution to Eq. (7.5) as we perform the deformation. For large Λ (and therefore, small r), the important terms in this equation are those that derive from varying $\mathcal{H}_{4\text{-deriv}}$, namely:

$$\frac{8 \sin^2 F_I(r)}{r^2} F_I''(r) - \frac{\sin 2F_I(r)}{r^2} \left(\frac{4 \sin^2 F_I(r)}{r^2} - 4F_I'(r)^2 \right) \approx 0. \quad (\text{A.7})$$

The key observation here is that this (approximate) equation is *scale invariant*, so that the solution in region I which satisfies the new perturbed boundary conditions, $F_I^{\text{new}}(0) = 0$ and $F_I^{\text{new}}(\Lambda^{-1}) = F_I((1-\eta)\Lambda^{-1})$, is just $F_I^{\text{new}}(r) \approx F_I((1-\eta)r)$ for all r in this range. A straightforward Taylor expansion then yields

$$\begin{aligned} H_I &\longrightarrow 4\pi \int_0^{\Lambda^{-1}} r^2 dr \mathcal{H}_{4\text{-deriv}} [F_I((1-\eta)r)] \\ &= 4\pi(1-\eta) \int_0^{(1-\eta)\Lambda^{-1}} \tilde{r}^2 d\tilde{r} \mathcal{H}_{4\text{-deriv}} [F_I(\tilde{r})] \\ &= 4\pi(1-\eta) \left\{ \int_0^{\Lambda^{-1}} \tilde{r}^2 d\tilde{r} \mathcal{H}_{4\text{-deriv}} [F_I(\tilde{r})] - \frac{\eta\Lambda^{-1}}{2e_S^2} \left(2F_I'^2 \sin^2 F_I + \Lambda^2 \sin^4 F_I \right) \right. \\ &\quad + \frac{1}{2!} \frac{\eta^2 \Lambda^{-2}}{2e_S^2} \left(2F_I'^3 \sin 2F_I + 4F_I' F_I'' \sin^2 F_I \right. \\ &\quad \left. \left. + 2\Lambda^2 F_I' \sin 2F_I \sin^2 F_I - 2\Lambda^3 \sin^4 F_I \right) \right. \\ &\quad - \frac{1}{3!} \frac{\eta^3 \Lambda^{-3}}{2e_S^2} \left(F_I'^4 (4 - 8 \sin^2 F_I) + 10F_I'^2 F_I'' \sin 2F_I \right. \\ &\quad \left. + 4(F_I' F_I''' + F_I''^2) \sin^2 F_I + \Lambda^2 F_I'^2 (12 \sin^2 F_I - 16 \sin^4 F_I) \right. \\ &\quad \left. \left. + (2\Lambda^2 F_I'' - 8\Lambda^3 F_I') \sin 2F_I \sin^2 F_I + 6\Lambda^4 \sin^4 F_I \right) + \mathcal{O}(\eta^4) \right\} \end{aligned} \quad (\text{A.8})$$

In the first equality we have changed integration variables to $\tilde{r} = (1-\eta)r$, and exploited the scale-covariance of $\mathcal{H}_{4\text{-deriv}}$.

This cumbersome expression simplifies considerably if one discards all terms of order Λ^0 , keeping only those of order Λ and $\Lambda^{1/2}$. At the point $r = \Lambda^{-1}$ where $F_I = F_{I\text{II}}$, the relevant scalings are

$$\begin{aligned} \frac{1}{2} \sin 2F_I &\approx (n + \frac{1}{2})\pi - F_I \sim \Lambda^{-1/2}, \quad \sin^2 F_I \approx 1, \\ F_{I\text{II}}' &\sim \Lambda^{1/2}, \quad F_I' \sim \Lambda, \quad F_I'' \sim \Lambda^{3/2}, \quad F_I''' \sim \Lambda^3 \end{aligned} \quad (\text{A.9})$$

thanks to Eqs. (8.1) and (A.7). Equation (A.8) collapses to

$$\begin{aligned}
H_{\text{I}} = 4\pi(1-\eta) & \left\{ \int_0^{\Lambda^{-1}} \tilde{r}^2 d\tilde{r} \mathcal{H}_{4\text{-deriv}}[F_{\text{I}}(\tilde{r})] - \frac{\eta\Lambda^{-1}}{2e_{\text{S}}^2} (2F_{\text{I}}'^2 + \Lambda^2) \right. \\
& + \frac{1}{2!} \frac{\eta^2\Lambda^{-2}}{2e_{\text{S}}^2} (2F_{\text{I}}'^3 \sin 2F_{\text{I}} + 4F_{\text{I}}'F_{\text{I}}'' + 2\Lambda^2 F_{\text{I}}' \sin 2F_{\text{I}} - 2\Lambda^3) \\
& - \frac{1}{3!} \frac{\eta^3\Lambda^{-3}}{2e_{\text{S}}^2} (-4F_{\text{I}}'^4 + 4F_{\text{I}}'F_{\text{I}}''' - 4\Lambda^2 F_{\text{I}}'^2 - 8\Lambda^3 F_{\text{I}}' \sin 2F_{\text{I}} + 6\Lambda^4) \\
& \left. + \mathcal{O}(\eta^4) + \mathcal{O}(\Lambda^0) \right\}. \tag{A.10}
\end{aligned}$$

Finally we consider region II, for which the deformation at short distances consists of adding the constant $F_{\text{I}}((1-\eta)\Lambda^{-1}) - F_{\text{I}}(\Lambda^{-1})$ to the right-hand side of Eq. (8.1). The dominant contribution to the energy in this region comes from the $\sin^4 F_{\text{II}}(r)/(2e_{\text{S}}^2 r^4)$ piece of Eq. (A.1), which is the only term whose integral diverges as $\Lambda \rightarrow \infty$. Another short exercise in Taylor expansion gives³¹

$$\begin{aligned}
H_{\text{II}} & \longrightarrow 4\pi \int_{\Lambda^{-1}}^{R_{\text{max}}} \frac{r^2}{2e_{\text{S}}^2 r^4} dr \sin^4 [F_{\text{II}}(r) + F_{\text{I}}((1-\eta)\Lambda^{-1}) - F_{\text{I}}(\Lambda^{-1})] \\
& = -\frac{2\pi}{e_{\text{S}}^2} \left[-\Lambda - 4\eta\Lambda^{-1}F_{\text{I}}'F_{\text{II}}' + 2\eta^2\Lambda^{-1}F_{\text{I}}'^2 \right. \\
& \quad \left. - \frac{\eta^3\Lambda^{-3}}{3!} (12\Lambda F_{\text{I}}'F_{\text{II}}'' + 4F_{\text{II}}'F_{\text{I}}''' - 4F_{\text{II}}'F_{\text{I}}'^3) \right] + \mathcal{O}(\eta^4) + \mathcal{O}(\Lambda^0). \tag{A.11}
\end{aligned}$$

The details of the upper limit of integration R_{max} are unimportant, as they do not conceivably involve divergent terms in Λ .

Assembling Eqs. (A.6), (A.10) and (A.11) yields the series expansion in the small-deformations parameter:

$$H_{\text{tot}}(\eta) = Z + \eta L + \eta^2 Q + \eta^3 C + \mathcal{O}(\eta^4). \tag{A.12}$$

Focusing first on the quantity of greatest interest, the quadratic coefficient Q , we find

$$Q = \frac{2\pi}{e_{\text{S}}^2} (\Lambda^{-2} F_{\text{I}}'^3 + F_{\text{I}}') \sin 2F_{\text{I}} + \mathcal{O}(\Lambda^0), \tag{A.13}$$

using Eq. (7.6) to eliminate $g_{\pi NN}^{\text{bare}}$. Notice that Q is only $\mathcal{O}(\Lambda^{1/2})$, the $\mathcal{O}(\Lambda)$ pieces having canceled between (A.10) and (A.11). This confirms Eq. (8.2).

³¹ The appearance of F_{II}' on the right-hand side is due to the observation that $\int_{\Lambda^{-1}}^{R_{\text{max}}} \frac{dr}{r^2} r^\lambda = \frac{d}{dr} r^\lambda \Big|_{r=\Lambda^{-1}} + \mathcal{O}(\Lambda^0)$ precisely when $\lambda = (1 \pm i\sqrt{3})/2$ as per Eq. (8.1).

The energy of this patched-together cloud is given by the zeroth-order coefficient Z :

$$\begin{aligned} Z &= 4\pi \int_0^{\Lambda^{-1}} \tilde{r}^2 d\tilde{r} \mathcal{H}_{4\text{-deriv}}[F_I(\tilde{r})] + \frac{2\pi}{e_S^2} \left(\Lambda - 4F_I F_I' + 4F_I F_{II}' \right) \\ &= \frac{2\pi}{e_S^2} \left(2\Lambda^{-1} F_I'^2 - 4F_I F_I' + 4F_I F_{II}' \right) + \mathcal{O}(\Lambda^0). \end{aligned} \quad (\text{A.14})$$

To eliminate the integral in the second equality, we have used the fact that since the cloud is a solution to Eq. (A.5) at $\eta = 0$, the linear term L must vanish:

$$0 = L = \frac{2\pi}{e_S^2 \Lambda} (2F_I'^2 - \Lambda^2) - 4\pi \int_0^{\Lambda^{-1}} \tilde{r}^2 d\tilde{r} \mathcal{H}_{4\text{-deriv}}[F_I(\tilde{r})] + \mathcal{O}(\Lambda^0). \quad (\text{A.15})$$

Numerically, Z turns out to be *negative definite* for the important case $n = 0$ in Eq. (8.1), corresponding to the coupling range $0 < g_{\pi NN}^{\text{ren}} < g_{\pi NN}^{\text{ANW}}$, as Z is then dominated by the attractive Yukawa contribution (A.4).

A nontrivial consistency check

Finally, the cubic coefficient is

$$C = \frac{4\pi}{3e_S^2 \Lambda^3} \left(F_I'^4 + \Lambda^2 F_I'^2 \right) + \mathcal{O}(\Lambda^{1/2}). \quad (\text{A.16})$$

The reason C is interesting is that there is a stringent consistency check on our calculations in terms of the ratio $R = Q/C$, which reads

$$F_I' \frac{\partial R}{\partial F_I} + F_I'' \frac{\partial R}{\partial F_I'} + F_I''' \frac{\partial R}{\partial F_I''} + \dots = -3\Lambda + \mathcal{O}(\Lambda^{1/2}). \quad (\text{A.17})$$

Thanks to Eq. (A.9), this is indeed satisfied by Eqs. (A.13) and (A.16).

To understand the source of this consistency check, look at Fig. 16. It shows that for every patched-together solution of the type we have been discussing, there must be another nearby solution, labeled “A” and “B”, respectively. Algebraically, this follows from the cubic polynomial (A.12), which can be rewritten more explicitly:

$$\begin{aligned} H_{\text{tot}}(\eta, \Lambda) &\cong Z(F_I(\Lambda^{-1}), F_I'(\Lambda^{-1}), \dots) + \eta^2 Q(F_I(\Lambda^{-1}), F_I'(\Lambda^{-1}), \dots) \\ &+ \eta^3 C(F_I(\Lambda^{-1}), F_I'(\Lambda^{-1}), \dots). \end{aligned} \quad (\text{A.18})$$

Aside from the starting solution “A,” which is at $\eta = 0$ by definition, Eq. (A.18) implies a new solution “B” which stationarizes $H_{\text{tot}}(\eta)$, at $\eta_* \cong -2R/3 \sim \Lambda^{-1/2}$. Alternatively, one could start one’s Taylor expansion at “B,”

$$\begin{aligned} H_{\text{tot}}(\eta, \Lambda) &\cong Z(F_I((1 - \eta_*)\Lambda^{-1}), F_I'((1 - \eta_*)\Lambda^{-1}), \dots) \\ &+ \eta^2 Q(F_I((1 - \eta_*)\Lambda^{-1}), F_I'((1 - \eta_*)\Lambda^{-1}), \dots) \\ &+ \eta^3 C(F_I((1 - \eta_*)\Lambda^{-1}), F_I'((1 - \eta_*)\Lambda^{-1}), \dots), \end{aligned} \quad (\text{A.19})$$

and demand that the original solution “A” be recovered at $\eta = \eta_{**}$. Consistency between these alternative starting points forces $1 - \eta_{**} = (1 - \eta_*)^{-1}$. When $\Lambda \gg 1$ so that η_* and $\eta_{**} \ll 1$, this in turn implies $\eta_{**} \cong -\eta_*$, or in other words,

$$R(F_I((1 - \eta_*)\Lambda^{-1}), F_I'((1 - \eta_*)\Lambda^{-1}), \dots) \cong -R(F_I(\Lambda^{-1}), F_I'(\Lambda^{-1}), \dots), \quad (\text{A.20})$$

whereupon Eq. (A.17) follows from a Taylor expansion in η_* .

A numerical example

Finally we describe a numerical example which bears out the above picture of “twinned” solutions “A” and “B,” and is further instructive in answering the question, What does the locally unstable cloud “A” collapse into?

Specifically, we have patched together a solution to Eq. (7.4) by fixing $g_{\pi NN}^{\text{ren}} = .65g_{\pi NN}^{\text{ANW}}$, and integrating Skyrme’s equation for $F_{\text{II}}(r)$ inwards from infinity, to a matching point at $r = \Lambda^{-1}$ where we fix $\Lambda = 6.5e_s f_\pi$. The “region I” curve $F_I(r)$ is then the solution to Skyrme’s equation with boundary conditions $F_I(0) = 0$ and $F_I(\Lambda^{-1}) = F_{\text{II}}(\Lambda^{-1}) = .68\pi$. From the slope discontinuity one finds $g_{\pi NN}^{\text{bare}} = 8.2e_s^{-2} f_\pi^{-1} = .46g_{\pi NN}^{\text{ANW}}$, while the total cloud energy (A.2) is $-183f_\pi/e_s$, which is within a few percent of the large- Λ approximation (A.14). Since at the matching point $F(\Lambda^{-1}) > \pi/2$, we expect this to correspond to the locally unstable configuration “A” in Fig. 16. Can one then uncover a solution with $F(\Lambda^{-1}) < \pi/2$, corresponding to the nearby locally stable (but still globally unstable) configuration “B”? Sure enough, for the same Lagrangian parameters Λ and $g_{\pi NN}^{\text{bare}}(\Lambda)$, one finds a second solution matched at $F(\Lambda^{-1}) = .41\pi$, whose renormalized coupling turns out to be tiny, $g_{\pi NN}^{\text{ren}} = .062g_{\pi NN}^{\text{ANW}}$, and whose total cloud energy is $-205f_\pi/e_s$, a little lower than that of “A” as Fig. 16 suggests.

Figure 16 further suggests the existence of a *third* solution, labeled “C,” which is energetically much more favorable than either “A” or “B.” We can argue for the necessity of such a solution, by noticing that for sufficiently negative η , eventually the cost in gradient energy must overwhelm the gain in the Yukawa interaction; therefore there must be a new minimum for some finite, negative η . One naturally guesses that this new solution looks more like the Skyrmion, meaning that the value of $F(\Lambda^{-1})$ is closer to π than $\pi/2$, and that the asymptotics of the tail is closer to Fig. 11. And indeed, for the same Lagrangian parameters, we have found a solution for which $F(\Lambda^{-1}) = 1.18\pi$, $g_{\pi NN}^{\text{ren}} = 1.08g_{\pi NN}^{\text{ANW}}$, and the total bag energy is $-338f_\pi/e_s$.

While we believe that, for this fixed choice of Λ , solution “C” is both a local and global minimum of the energy, certainly if it is extrapolated far enough into the ultraviolet with

the large- N_c renormalization group, it too eventually develops an instability. Although we have not pushed the numerics, it is tempting to conjecture that the cloud then collapses to one whose renormalized coupling is closer still to $g_{\pi NN}^{\text{ANW}}$, and that by continuing in this way—alternating RG flow with cloud collapse to a new renormalized coupling, followed by renewed RG flow to still higher Λ , and so forth—one iterates one's way to $g_{\pi NN}^{\text{ANW}}$ precisely.

References

- [1] T. H. R. Skyrme, *Proc. Roy. Soc.* **A260** (1961) 127; *Nucl. Phys.* **31** (1962) 556.
- [2] G. Adkins, C. Nappi and E. Witten, *Nucl. Phys.* **B228** (1983) 552.
- [3] G. 't Hooft, *Nucl. Phys.* **B72** (1974) 461 and **B75** (1974) 461.
- [4] A classic review is J. Kogut and K. Wilson, *Phys. Rep.* **12**, No. 2 (1974) 75.
- [5] N. Dorey, J. Hughes and M. Mattis, *Phys. Rev. Lett.* **73** (1994) 1211.
- [6] N. Dorey, J. Hughes and M. Mattis, *Phys. Rev.* **D50** (1994) 5816.
- [7] G. Veneziano, *Nucl. Phys.* **B117** (1976) 519.
- [8] E. Witten, *Nucl. Phys.* **B160** (1979) 57.
- [9] P. Arnold and M. Mattis, *Phys. Rev. Lett.* **65** (1990) 831; M. Mattis and R. Silbar, *Phys. Rev.* **D** (in press).
- [10] A. Chodos and C. Thorn, *Phys. Rev.* **D12** (1975) 2733.
- [11] M. Rho, A. S. Goldhaber and G. E. Brown, *Phys. Rev. Lett.* **51** (1983) 747.
- [12] J. Goldstone and R. L. Jaffe, *Phys. Rev. Lett.* **51** (1983) 1518.
- [13] An excellent recent review of chiral bags and Cheshire cats is M. Rho, *Phys. Rep.* **240** (1994) 1.
- [14] J. Gervais and B. Sakita, *Phys. Rev.* **D30** (1984) 1795.
- [15] S. Nadkarni, H. Nielsen, and I. Zahed, *Nucl. Phys.* **B253** (1985) 308; P.H. Damgaard, H.B. Nielsen and R. Sollacher, *Nucl. Phys.* **B385** (1992) 227 and *Phys. Lett.* **B296** (1992) 132.
- [16] S. Coleman, *Phys. Rev.* **D11** (1975) 2088; S. Mandelstam, *Phys. Rev.* **D11** (1975) 3026.
- [17] A. Manohar, *Phys. Lett.* **B336** (1994) 502.
- [18] G. H. Derrick, *J. Math. Phys.* **5** (1964) 1252; R. Hobart, *Proc. Royal. Soc. London* **82** (1963) 201.
- [19] M. A. Luty and J. March-Russell, *Nucl. Phys.* **B426** (1994) 71; M. A. Luty, hep-ph/9405271; M. A. Luty, J. March-Russell and M. White, hep-ph/9405272.
- [20] C. Carone, H. Georgi and S. Osofsky, *Phys. Lett.* **B322** (1994) 227; C. Carone, H. Georgi, L. Kaplan and D. Morin, *Phys. Rev.* **D50** (1994) 5793.
- [21] M. Mattis and M. Mukerjee, *Phys. Rev. Lett.* **61** (1988) 1344.
- [22] A. V. Manohar, *Nucl. Phys.* **B248** (1984) 19.
- [23] M. Mattis and E. Braaten, *Phys. Rev.* **D39** (1989) 2737.
- [24] R. Dashen, E. Jenkins and A. V. Manohar, hep-ph/9411234.
- [25] M. Mattis, *Phys. Rev.* **D39** (1989) 994; *Phys. Rev. Lett.* **63** (1989) 1455.
- [26] R. Dashen and A. V. Manohar, *Phys. Lett.* **B315** (1993) 425 and 438; R. Dashen, E. Jenkins and A. V. Manohar, *Phys. Rev.* **D49** (1994) 4713; E. Jenkins and A. V. Manohar, *Phys. Lett.* **B335** (1994) 452.
- [27] E. Jenkins, *Phys. Lett.* **B315** (1993) 441.

- [28] See for example T.-S. H. Lee and F. Tabakin, *Nucl. Phys.* **A191** (1972) 332, Table 1; V. Barger and M. Ebel, *Phys. Rev.* **138** (1965) B1148; R. Machleidt, K. Holinde and Ch. Elster, *Phys. Rep.* **149** (1987) 1; and M. Lacombe *et al.*, *Phys. Rev.* **C21** (1980) 861.
- [29] A. Hayashi, G. Eckart, G. Holzwarth and H. Walliser, *Phys. Lett.* **B147** (1984) 5.
- [30] M. Mattis and M. Peskin, *Phys. Rev.* **D32** (1985) 58; M. Karliner, *Phys. Rev. Lett.* **57** (1986) 523.
- [31] M. Mattis, *Phys. Rev. Lett.* **56** (1986) 1103.
- [32] L. S. Schulman, *Phys. Rev.* **176** (1968) 1558; and *Techniques and Applications of Path Integration*, (Wiley-Interscience 1981).
- [33] D. Diakonov, *Acta Phys. Pol.* **B25** (1994) 17; D. Diakonov and V. Petrov, St. Petersburg preprint LNPI-1394, 1988 (unpublished).
- [34] E. Guadagnini, *Nucl. Phys.* **B236** (1984) 35.
- [35] B. J. Schroers, *Zeit. Phys.* **C61** (1994) 479; Sec. 3.
- [36] B. Schwesinger, H. Weigel, G. Holzwarth and A. Hayashi, *Phys. Rep.* **173** (1989) 173; and references therein.
- [37] A. Jackson, A. D. Jackson, and V. Pasquier, *Nucl. Phys.* **A432** (1985) 567.
- [38] B. Piette, H.. Müller-Kirsten, D. Tchraikian and W. Zakrzewski, *Phys. Lett.* **B320** (1994) 294; B. Piette, B. Schroers and W. Zakrzewski, hep-th/9406160, to appear in *Zeit. Phys.* **C**, and hep-ph/9410256.
- [39] For a review and references to the literature on the $O(3)$ σ model, see V. Novikov, M. Shifman, A. Vainshtein and V. Zakharov, *Phys. Rep.* **116** (1984) 103. A solution of the two-dimensional model is given by P. Wiegmann, *Phys. Lett.* **152B** (1985) 209.
- [40] B. S. Balakrishna, V. Sanyuk, J. Schechter and A. Subbaraman, *Phys. Rev.* **D45** (1992) 344; Sec. II.

Figure Captions

Contact mattis@skyrmion.lanl.gov for hard copies
if you cannot process the figures from hep-ph

1. Three types of large- N_c models of the strong interactions, and the relationships between them. This paper examines two of the three arrows, Effective QFT \implies “Chiral bags,” and “Chiral bags” \implies Skyrmons. The third relation, Skyrmons \implies Effective QFT, is examined in depth in Ref. [6].

2. (a) A bare meson-baryon coupling $g_{\text{bare}} \sim \sqrt{N_c}$, which we shall refer to generically as a “Yukawa coupling” even if it involves derivatives. Henceforth, directed lines are baryons, undirected lines are mesons. (b) A simple radiative correction to (a). Since the 3-meson vertex $\sim 1/\sqrt{N_c}$, this graph too $\sim \sqrt{N_c}$. Therefore, it is a leading-order contribution to g_{ren} . (c) A more complicated contribution to g_{ren} which is likewise leading-order. The general rule is: the leading-order graphs are the ones for which, if one erases the baryon line(s), one is left with meson tree(s). (d) An example of a subleading contribution to g_{ren} . The purely mesonic loop costs one power of N_c , so this graph $\sim 1/\sqrt{N_c}$.

3. (a) A “seagull” interaction, in which more than one meson interacts with the baryon at the same space-time point. The ellipses allow for yet more meson lines than shown meeting at the vertex. (b) A Z -graph, in which the baryon runs backwards in time over an interval. These arise in the decomposition of Feynman graphs into time-ordered diagrams. Time runs upwards in this diagram. (c) An effective seagull, or “ Z -gull,” implied by (b). For Yukawa couplings that obey the $I_t = J_t$ rule, (c) is suppressed by $1/N_c^2$ compared to the bare seagull shown in (a).

4. The complete set of leading-order corrections of the type shown in Figs. 2a-c. The oval blob is understood to contain all tree-level meson branchings (no loops). There is an explicit sum over the $n!$ attachments of the blob to the baryon line.

5. The graphical Born-series solution of Eq. (3.2). The line terminating in a square is our notation for $\vec{\pi}_{c1}$, the oval blob contains all tree-level meson branchings, and the Yukawa source \mathcal{Y} is short for the right-hand side of Eq. (3.2).

6. An equivalent rewrite of Fig. 5, with the baryon explicitly drawn (it is implicit in the Yukawa source of Fig. 5). The difference with Fig. 4 lies solely in the time-ordering up the baryon line (a $1/N_c$ difference).

7. (a) The left-hand side of Eq. (3.5), formed from Eqs. (2.8) and (3.1), in the graphical language of Fig. 5. The third summand stands for the sum of all the vertices in the potential $V(\vec{\pi}_{c1})$. Varying (a) with respect to $\vec{\pi}_{c1}$ gives Eq. (3.2). (b) Born-series rewrite of (a) using the expansion shown in Fig. 5, with combinatoric factors suppressed. (c) The meaning of (b) as baryon self-energy and meson-baryon vertex corrections, interpreted in the original Feynman-diagrammatic language of Fig. 2. These corrections, shown to the right of the baryon line, need to be inserted in all possible locations up this line, as dictated by Eq. (3.3).

8. Typical hedgehog profile $F(r)$. In the large- r regime, all the complicated dependence on the meson potential $V(\vec{\pi})$ and on the form of the regulator $\delta_\Lambda(r)$ has been reduced to the single parameter $g_{\pi NN}^{\text{ren}}$ which measures the height of the tail.

9. Construction of the patched-together cloud $F(r) = \theta(\Lambda^{-1} - r)F_I(r) + \theta(r - \Lambda^{-1})F_{II}(r)$ for the model of Sec. 5. (a) The curve $F_{II}(r)$, which is uniquely specified by the asymptotic form, Eq. (3.17). The x axis is in units of the $\mathcal{O}(N_c^0)$ length $(3g_{\pi NN}^{\text{ren}}/2\pi f_\pi)^{1/2}$. $F_{II}(r)$ blows up like $1/r$ for small r . (b) The curve $F_I(r)$. The cross indicates the curve's maximum, $F_I^{\text{max}} \cong .58\pi$. (We have also marked by a cross in (a) the point where $F_{II}(r) = F_I^{\text{max}}$ which defines the critical scale $r = \Lambda_2^{-1}$ discussed in the text.) In Region A its slope is positive and in Region B it is negative; eventually the curve asymptotes to $\pi/2$. The scale of the x axis is purposefully not displayed, because this curve stands for the entire one-parameter *family* of curves related by dilatations: $F_I(r) \rightarrow F_I(\lambda r)$. For any given value of the cutoff Λ , this λ is to be adjusted so that $F_I(\Lambda^{-1}) = F_{II}(\Lambda^{-1})$.

10. The patched-together solution to Eq. (6.14), namely: $F(\tilde{r}) = 2\text{Tan}^{-1}(\tilde{\Lambda}^2\tilde{r})\theta(\tilde{\Lambda}^{-1} - \tilde{r}) + (\pi - 2\text{Tan}^{-1}\tilde{r})\theta(\tilde{r} - \tilde{\Lambda}^{-1})$, where the dimensionless variables are $\tilde{r} = 4\pi f r/g_{\text{ren}}$ and $\tilde{\Lambda} = g_{\text{ren}}\Lambda/4\pi f$. Shown is the curve for $\tilde{\Lambda}^{-1} = 4$.

11. The original Skyrmeon [1,2]. The x axis is in $\mathcal{O}(N_c^0)$ length units $(e_s f_\pi)^{-1}$.

12. (a) A generic bare 3-meson vertex. (b) and (c): Radiative corrections to the vertex, both of which are down by $1/N_c$ compared to (a), thanks to selection rule **(i)** in Sec. 2.1. Hence, unlike Yukawa couplings, purely mesonic vertices do *not* run in the large- N_c renormalization group at leading order. It is therefore reasonable to fix the bare mesonic parameters to the experimental data at the outset.

13. Family of curves $F_I(r)$ that solve Skyrme's equation. When $g_{\pi NN}^{\text{ren}} \equiv g_{\pi NN}^{\text{ANW}}$, $F_{II}(r)$ is just the Skyrmeon profile shown in Fig. 11.

14. (a) A typical curve $F_{II}(r)$ when $0 < g_{\pi NN}^{\text{ren}} < g_{\pi NN}^{\text{ANW}}$. As explained in the text, rather than approaching π for small r , this curve spirals into $\pi/2$. The x axis is in units $(e_s f_\pi)^{-1}$. (b) The short-distance behavior of (a) in logarithmic variables, confirming the oscillatory behavior of Eq. (8.1). The variable plotted on the x axis is $\log(e_s f_\pi r)$, while the y axis is $(e_s f_\pi r)^{-1/2}(F_{II} - \pi/2)$ as suggested by Eq. (8.1).

15. A dangerous small deformation of the patched-together pion cloud. For alternating regions in Λ , the cloud energy proves to be quadratically unstable against this deformation, and the cloud instantly collapses to another configuration closer to the Skyrmeon. The deformation is defined as follows. Hold the matching point fixed at $r = \Lambda^{-1}$, but raise the value of $F_I(\Lambda^{-1}) = F_{II}(\Lambda^{-1})$ infinitesimally, while letting the entire curve $F_I(r)$ relax to a new solution of Eq. (7.5) for $r < \Lambda^{-1}$. For $r \gtrsim \Lambda^{-1}$, raise $F_{II}(r)$ by a constant amount so that the curves stay matched, then merge this curve smoothly to an r^{-2} falloff at large distances (the details of this merging are irrelevant for sufficiently large Λ).

16. Total cloud energy H_{tot} as a function of the matching-point value $F_I(\Lambda^{-1}) = F_{II}(\Lambda^{-1})$. For large Λ , the existence of nearby solutions "A" and "B" follows from the cubic

polynomial, Eq. (A.12), remembering that $L = 0$, $Q = \mathcal{O}(\Lambda^{1/2})$, and $C = \mathcal{O}(\Lambda)$, and that the sign of Q depends on whether $F(\Lambda^{-1})$ is greater or less than $\pi/2$. As Λ increases further, “A” and “B” exchange relative positions every half period in the sinusoidal oscillations of Eq. (8.1). Numerical evidence for the global minimum solution “C,” nearer the Skyrmion, is presented in the text.

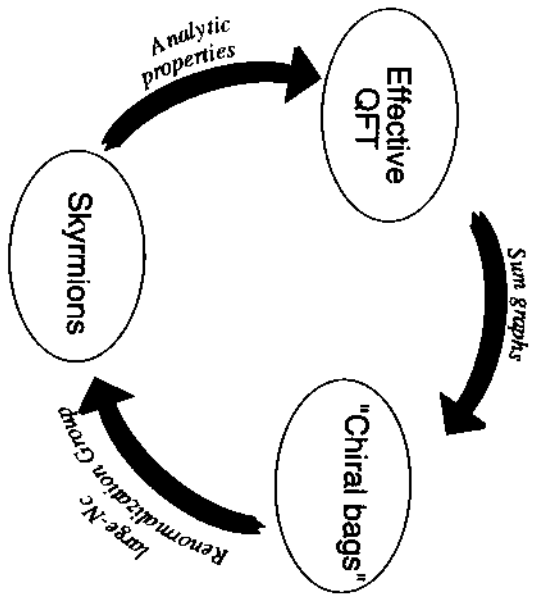


Fig. 1

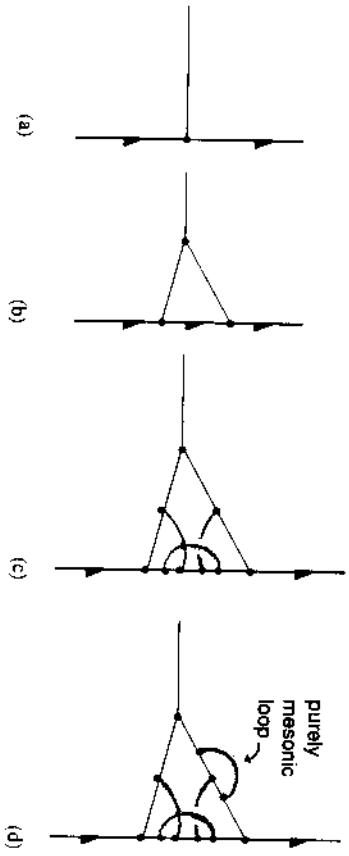


Fig. 2

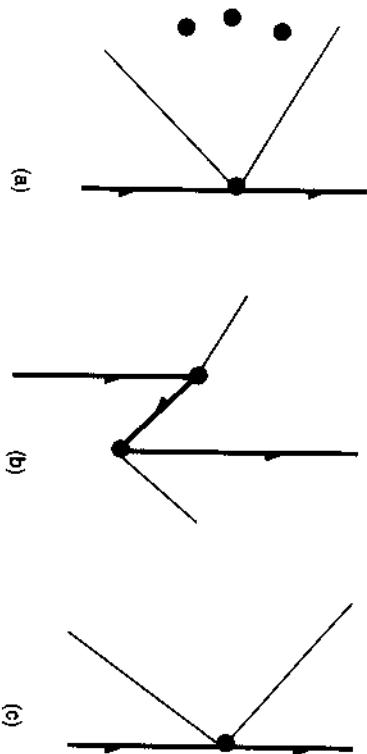


Fig. 3

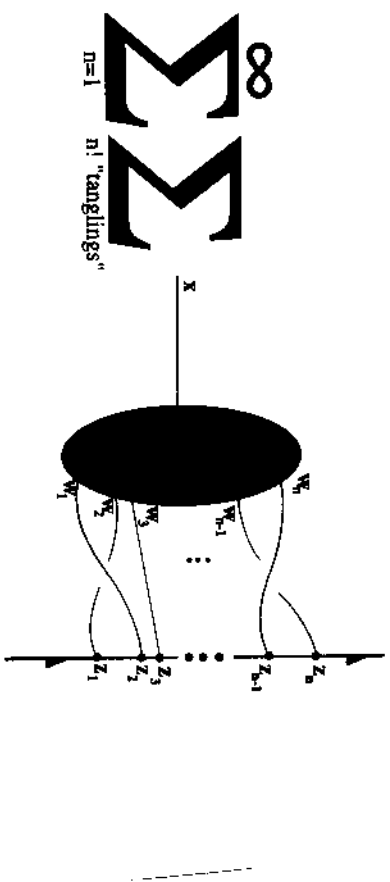


Fig. 4

$$\pi_n(x) = x \cdot y(z_1) + x \cdot y(z_2) + \dots$$

$$= \sum_{n=1}^{\infty} x \cdot y(z_n)$$

Diagram illustrating a summation over $n!$ "tangles". The diagram shows a horizontal axis with points $z_1, z_2, z_3, \dots, z_{n-1}, z_n$. A black oval is positioned above the axis. Wavy lines connect the points $z_1, z_2, z_3, \dots, z_{n-1}, z_n$ to the oval, representing different tangles. The summation is labeled $\sum_{n=1}^{\infty} n!$ "tangles".

Fig. 5

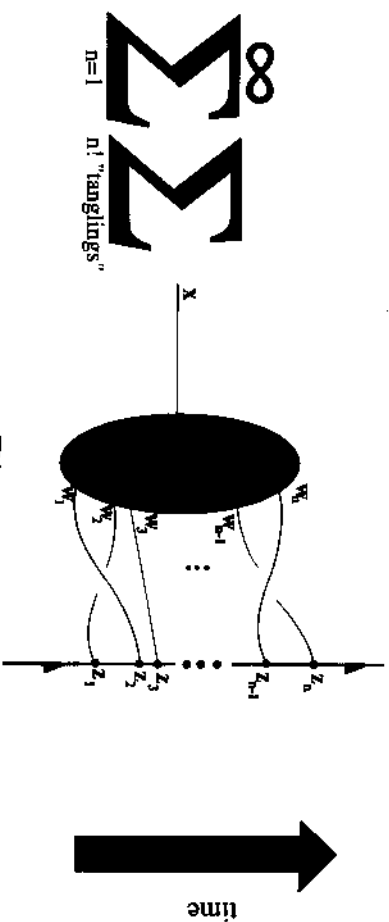
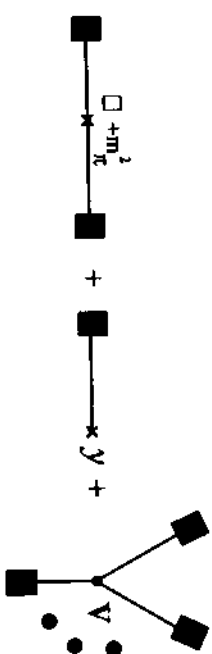
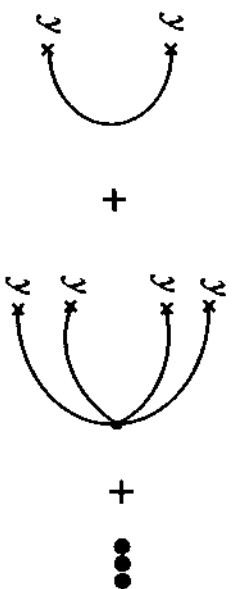


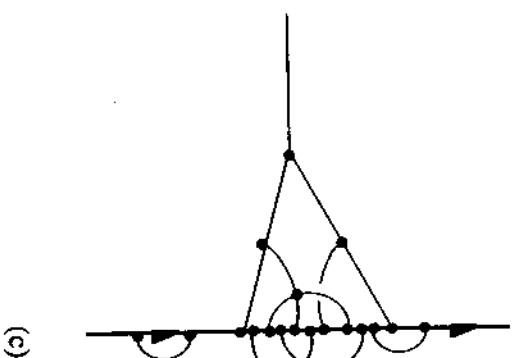
Fig. 6



(a)



(b)



(c)

Fig. 7

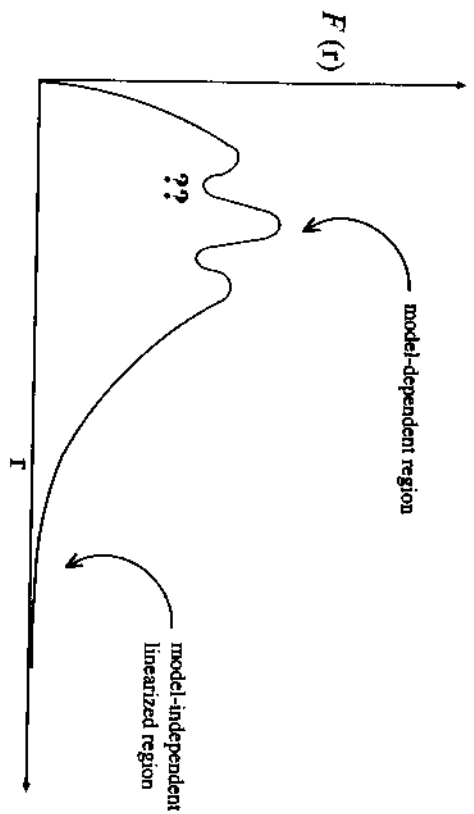
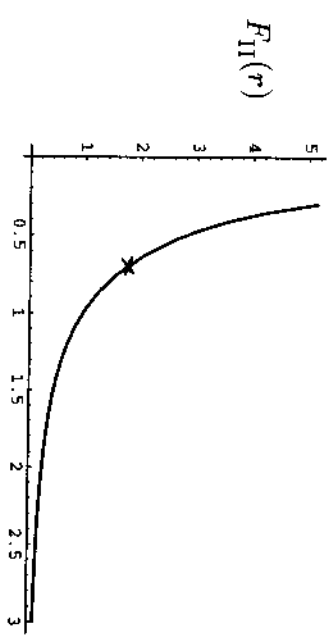
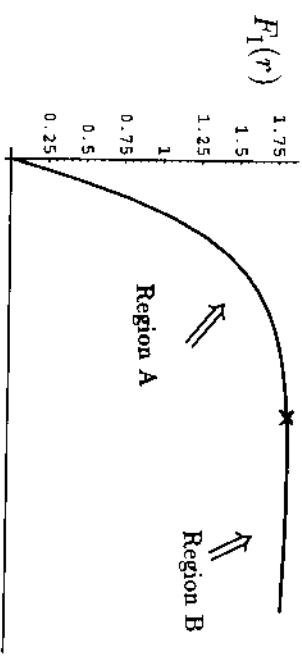


Fig. 8



(a)



(b)

Fig. 9

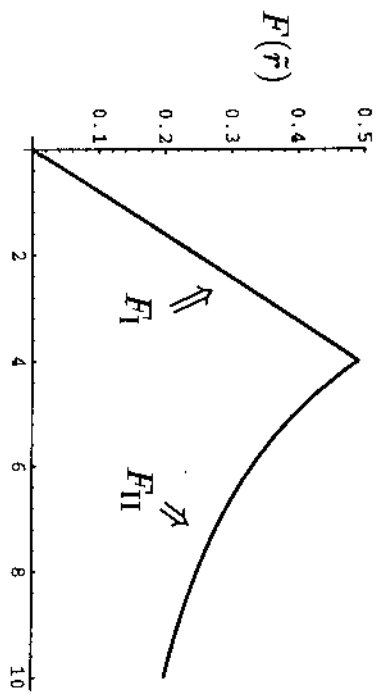


Fig. 10

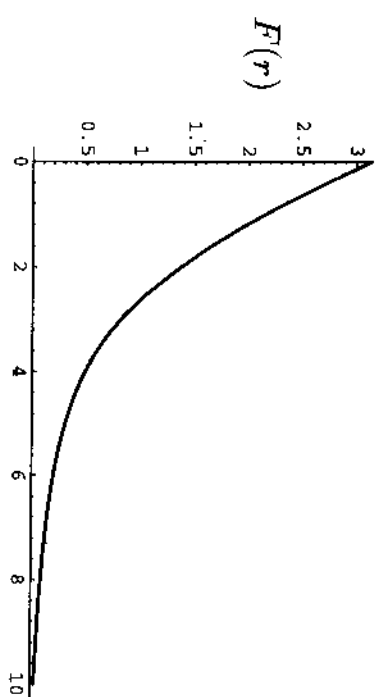


Fig. 11

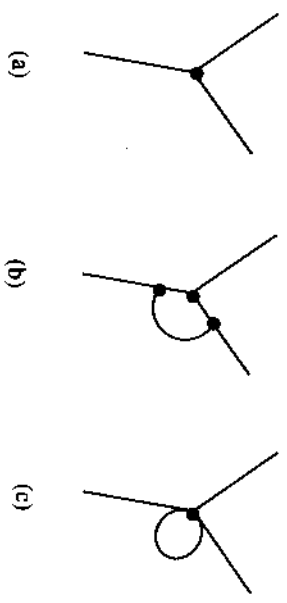


Fig. 12

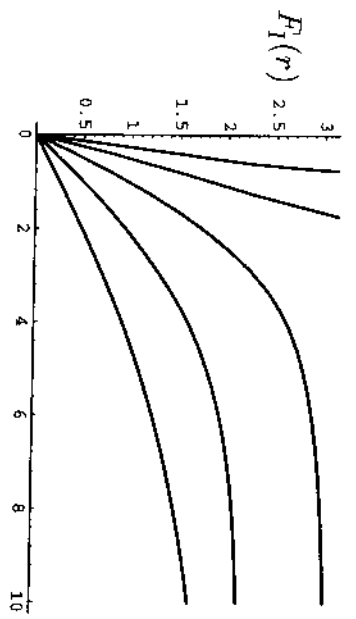
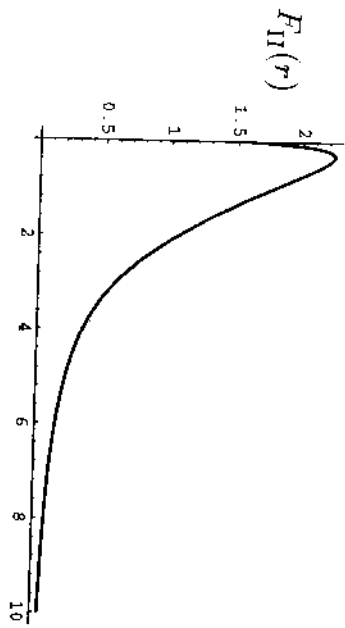
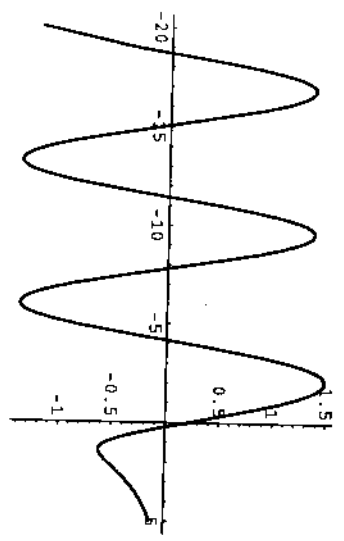


Fig. 13



(a)



(b)

Fig. 14

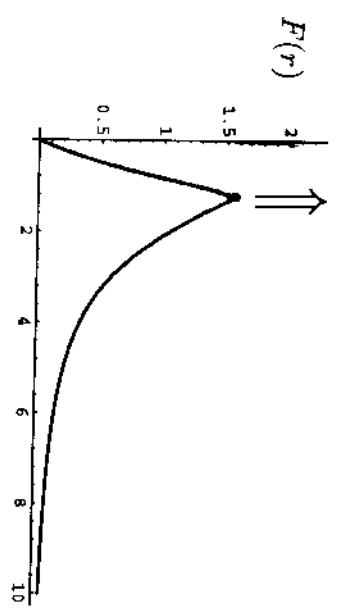


Fig. 15

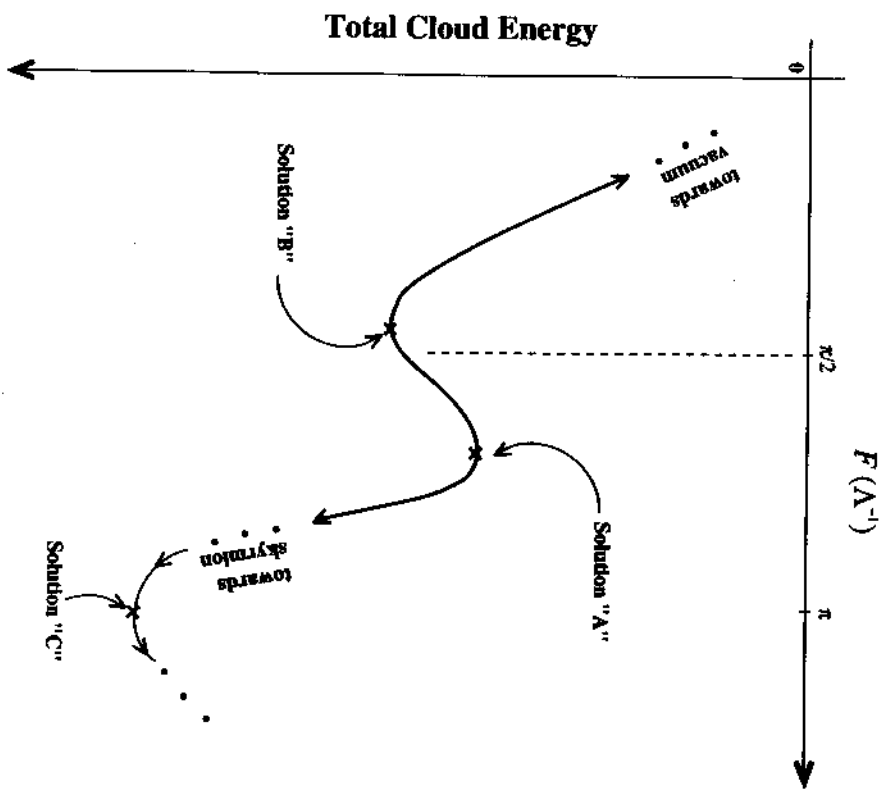


Fig. 16

This figure "fig1-1.png" is available in "png" format from:

<http://arxiv.org/ps/hep-ph/9412373v2>

This figure "fig1-2.png" is available in "png" format from:

<http://arxiv.org/ps/hep-ph/9412373v2>

This figure "fig1-3.png" is available in "png" format from:

<http://arxiv.org/ps/hep-ph/9412373v2>

This figure "fig1-4.png" is available in "png" format from:

<http://arxiv.org/ps/hep-ph/9412373v2>